Department of the Navy
Naval Ordnance Test Station
Contract N123(60530)34767A

SUPERVENTILATED FLOW PAST DELTA WINGS

by

Taras Kiceniuk

Hydrodynamics Laboratory
Karman Laboratory of Fluid Mechanics and Jet Propulsion
California Institute of Technology
Pasadena, California

Report No. E-101.5 July 1964

NOMENCLATURE

Symbols	Definition	Units
L	Length of model	Ft
A	Plan form area of model in Ft^2	Ft^2
x	Longitudinal distance along model, upstream from trailing edge	Ft
z	Transverse distance on model, from model centerline	Ft
z_x	Half-breadth of model at longitudinal position x	Ft
Y_o	Submergence measured vertically from undisturbed free surface	Ft
Y^*	Submergence measured to model centroid	Ft
$\bar{x}$	Longitudinal distance to center of pressure	Ft
z_{max}	Half-breadth of model at widest point	Ft
γ	Model total apex angle	Degrees
α	Model angle of attack	Degrees
p_o	Free stream static pressure	Lbs/Ft^2
p_k	Cavity pressure	Lbs/Ft^2
h_o	Free stream static head measured relative to atmosphere	Ft of water
h_k	Cavity pressure measured relative to atmosphere	Ft of water
ρ	Mass density of water	Slugs/Cu Ft

NOMENCLATURE (continued)

Symbols	Definition	Units
g	Acceleration of gravity	Ft/Sec^2
V_o	Free stream velocity	Ft/Sec
$K = \frac{p_o - p_k}{\frac{1}{2} \rho V_o^2}$	Cavitation or ventilation number	Dimensionless
$C_L = \frac{Lift}{\frac{1}{2} \rho V_o^2 A}$	Lift coefficient	Dimensionless
$C_D = \frac{Drag}{\frac{1}{2} \rho V_o^2 A}$	Drag coefficient	Dimensionless
$C_M = \frac{Moment\ (t.e.)}{\frac{1}{2} \rho V_o^2 A L}$	Moment coefficient about trailing edge	Dimensionless

Introduction

Although delta wings have been known for some time in aeronautics[1][2]* their introduction into a hydrodynamic context has been quite recent. As in the flow of air, the delta wing provides a simple but useful configuration for investigating three-dimensional problems in cavity flows. At the start of the present work (1960), only one theoretical study on this subject was known[3]. No information on flow patterns, force characteristics or other properties were available for these shapes. It was accordingly decided to embark on an experimental program with the aim of providing the basic characteristics of the cavitating flow past delta wings, to observe and outline any interesting features of these flows and, finally, to provide a physical basis for any mathematical analysis of the flow that might be undertaken. Measurements of lift, drag and pitching moment and pressure distributions were made on a family of simple flat plate delta shapes of varying apex angle; several configurations outside this family were also tested. These included a diamond plan form, reverse delta, and a delta with a 90 degree bottom. All were without camber and were tested with no yaw angle.

After completion of this work, the exhaustive treatment of Reichardt and Sattler[4] appeared which also deals with cavitating delta wings. It is believed, however, that the current report and that of Reichardt are sufficiently different in scope and method to justify the presentation of the present results.

Instruments and Apparatus

The experimental program described in this report was performed in the Free-Surface Water Tunnel at the California Institute of Technology.[5] The working section of this tunnel, shown diagrammatically in Figure 1, permits force and pressure measurements to be made at velocities up to 27 fps in the presence of a free water surface. The boundary layer skimmer located at the upstream end of the working section, removes the slow-moving top layer of water in the nozzle. The resulting velocity profile, labeled B in Figure 1, shows no perceptible variation except at the lower boundary and side walls of the 20 inch by 20 inch working section.

---

*Numbers in parenthesis refer to references at end of text.

The forces and moment acting on the model were measured on the three-component force balance. This balance, described in greater detail in Reference 6, is an electrical-mechanical type to which the model is attached by means of a shielded adjustable strut assembly. Simultaneous readings of forward lift, rear lift, and drag are combined by a simple computational procedure into lift, drag, and pitching moment coefficients, the latter being taken about the trailing edge of the model. The elevating mechanism to which this balance is attached can be raised or lowered so that the model can be completely submerged, or it can be raised through the free surface and out of the moving water.

The support-strut assembly consists of an inner support strut and an outer streamlined fairing. Within the fairing are contained the tubes which supply air to the cavity and which permit the cavity pressure to be measured. No mechanical seal is provided between the cavity bubble and the outside air above the water surface, a condition which might have resulted in the maximum cavity pressure being limited by the leakage of air from within the cavity. To obviate this possibility, preliminary experiments were made using a water seal, in which a generous external supply of water at low pressure was permitted to fill the space between the fairing and the support strut. Although this seal worked very well, it was found to be unnecessary since the rate of air loss past the strut was found to be small compared to the air entrainment at the downstream end of the cavity.

The angle of attack of the model could be changed during the course of the run by means of the adjusting knob located at the upper end of the strut, but was limited to an excursion of plus or minus 10 degrees from the pre-set midpoint. The dial indicator, reading in thousandths of an inch, had previously been calibrated to indicate angle of attack. This dial indicator can be seen in Figure 2 which shows a slender delta wing and the lower end of the force balance during a typical run at moderate submergence. The lower end of the support strut fairing and the point of attachment at the model were not faired since they did not contact moving water inside the air supported cavity.

The supplementary air supply probe can be seen in these same photographs, extending upstream from its surface-piercing support strut to its terminating point within the cavity. This supplementary supply was used only to check whether or not the upper value of cavity pressure was being limited by the air supply rate obtainable through the piping within the strut fairing. When it was conclusively proved that this was not the case, the auxiliary air supply was removed and the air supply lines within the model support strut fairing were used alone.

The pressure in the cavity was measured on a water manometer since the range of cavity pressures usually encountered in air supported cavities of this type are within a foot or two of atmospheric pressure for velocities less than 25 fps. In order to make sure that the pressure tap line was free of water at all times, some air was continually bled into the cavity space through the pressure measuring tap. The pressure drop associated with this small air flow rate through the pressure line causes the cavity pressure manometer to read about .01 feet too high. This error was easily compensated for by adjusting the scale at the start of the run by first raising the model out of the water and using the ambient air pressure as the known zero pressure reference.

Description of Models

The design requirement of each model was that it be hydrodynamically equivalent to a flat plate, wetted only on the pressure side and not contacting the cavity wall on its upper surface. This goal could be met easily and inexpensively by machining the model from flat aluminum stock beveled 45 degrees along the sides of the hydrofoil. If handled carefully the edges remain reasonably sharp, and preliminary tests proved that the model did not deform under the influence of the hydrodynamic loads. The plates were made in thicknesses that varied from 1/8 inch to 1/4 inch, depending upon the strength and deflection requirements imposed by the particular geometry and point of support. The models tested, as well as critical dimensions, are shown in Figure 3. Provisions for making pressure distribution surveys of the 15 degree model consisted of 1/16 inch diameter piezometer openings distributed at key points along the bottom of the model, communicating to

flexible polyethylene tubing by means of the short lengths of bent brass tubing which can be seen in Figure 3(a). The piezometer openings were made large in the interest of increasing the response time of the pressure measuring system. Smaller openings would have been used had the pressure not been measured on the large-bore multi-manometers. The same pressure tap openings were also used for flow visualization purposes by connecting the thin polyethylene tubing to a low pressure source of water which had previously been colored by dissolving potassium permanganate in it.

Figure 3(a) also shows the brass tubing from which a jet of colored water was discharged into the bubble wall near the tip of the model. Cotton tufts also were employed for flow visualization. The model was prepared by drilling small holes in the bottom, then counter-boring these holes with a larger diameter drill from the upper or "suction" side. In this way a short length of string knotted at the end, could be inserted through the model and held in place by a plug of wax pressed against the knot at the base of the larger diameter hole in the upper surface. This method was deemed preferable to gluing the tufts to the model surface itself since the thread protrudes normal to the model surface and is, therefore, free to assume any flow direction without initial bias.

At the extreme forward tip of the model close examination during preliminary runs showed that the water flowed around the sharp edge of the model, clinging to the upper surface of the model for a distance of as much as 1/2 inch before springing free at the sharp edge! Since the models had been made of aluminum, and since no particular care had been taken to achieve an extremely sharp edge on the model, it was felt that fabrication defects, combined with the low Reynolds number which existed near the extreme tip, produced this disparity from the ideal flow. It was believed that this wetting of the model tip might also account for the clinging of the septum which could be observed along the entire upper surface of the model at angles of attack less than 21 degrees for all of the deeply submerged models. Similar to the "teapot" effect, the septum would cling or spring free under the influence of small flow fluctuations near this minimum angle. The wetting of the upper surface of the model by the septum did not noticeably affect the forces acting on the model because the septum was

extremely thin, but it had been hoped to achieve the lowest possible angles of attack and still maintain the bubble geometry as presented in Figure 4. For this reason a model was made from stainless steel with edges accurately lapped to a razor edge to the extreme tip, a refinement which could not be achieved on the more fragile aluminum models. Both for convenience of fabrication and for the purpose of exploring another model geometry, the upper surface of this model (Model 3A, Figure 3) was made V-shaped with a dihedral angle of 90 degrees.

These attempts resulted in no noticeable reduction in minimum angles of attack and the upper surface of the tip of this model was wetted to the same extent as were those made from aluminum. The water viscosity and surface tension appear to control the flow in this region, where the Reynolds number (based on free stream velocity and distance from the tip) is approximately 15,000.

Another attempt to reduce the angle of attack at which superventilated flow could be achieved was made by blunting the model tip. As expected, this change in model shape had the effect of causing a local cavity to spring from the tip much the same as it would behind a flat disc, in the immediate vicinity of the model tip. The effects of this small cavity disappeared within an inch or so and the remainder of the cavity bubble appeared the same as did those with sharp tips. A small reduction in the minimum angle of attack was achieved before giving rise to the before-mentioned "teapot" effect, but the gain was limited to one or two degrees and this scheme was abandoned.

A possible defect of the model support system was that the deflection of the model and support strut could result in a change in angle of attack of the model. To check this possibility the models and support systems were fastened to a heavy surface plate and loads were applied equal to those measured during the run. The resulting deflections were measured and recorded. All data presented in this report have been corrected for model deflection, even though that model deflection was, in nearly all cases, less than 1/10 of a degree.

Selection of Model Size

The choice of model size was dictated by the following considerations:

1. The model must be small enough so that tunnel blockage will not noticeably affect the forces or the shape of the cavity.
2. The model size must be compatible with the force range of the available balance system. The upper limit of these forces is 10 pounds for the electrical-mechanical balance, whereas the lower limit is set, not by the accuracy of the balance, but by the dimensions of the model support system. If the model is made too small, the cavity bubble produced by it is not large enough to envelop the existing strut support fairing, with the result that spray strikes the model.
3. The model must be large enough to show no velocity scaling effects. If the model is made too small it can be expected that viscosity and surface tension effects will play a large role in determining the flow configuration, whereas models which are too large will be operating at a sufficiently low Froude Number, for gravity effects to be important.

The final verification of correct model size was based on the preliminary experiments using delta wings with an apex angle of 15 degrees. Models 11.2 inches long and 8.28 inches long were tested and found to exhibit identical flow geometries and lift and drag coefficients. The smaller one was chosen for the reasons enumerated above. The area of this model was $0.063\,ft^2$. The models with apex angle other than 15 degrees were made approximately equal in plan form area.

Observations and Flow Visualization

Before placing the superventilated delta wing in the water tunnel it was not known what the resulting flow and bubble configuration would be. Results of tests performed in air[2], and therefore corresponding to the fully-wetted flow, indicated that a pair of vortices would form along the edges of the delta wing and trail downstream. Exactly what would become of these vortices at cavitation numbers low enough to result in supercavitation or superventilation was a matter for conjecture. A plausible guess was that a large simple bubble such as the one assumed by Cumberbatch and Wu[7] would envelop the upper surface of the hydrofoil and extend several chords

downstream. The actual bubble geometry observed was strikingly different from the expected one. First, it became apparent that moderate angles of attack were necessary to achieve completely superventilated flow, in which the upper surface of the model was not touched by the water. At angles of attack greater than 21 degrees, with moderate quantities of air supplied in the wake of the model, a clear single bubble was obtained. The appearance of this bubble is best shown by the sketch in Figure 4, although critical examination of Figure 2 and other photographs appearing in this report reveals the same distinguishing features.

The drawing in Figure 4 is a composite made from many photographs and sketches and is intended only to demonstrate the general features of the flow rather than specific details associated with particular operating conditions. Accurate survey techniques were not used to determine the shape of the bubble cross-section and so it must be regarded as an artist's sketch only. The lines in the drawing represent the flow direction as determined by dye streak photographs and by photographs of the tufts on the model. The angles depicted in the side view show how the flow begins to deviate from being purely conical as the base of the model is approached.

Starting with the fully-wetted hydrofoil, and gradually increasing the quantity of air which is bled into the wake region aft of the hydrofoil, thin frothy tip vortices became visually apparent as air was drawn into vortex cores. Force measurements could not be accurately made with the existing strut and shield assembly for this flow condition since the model support structure was directly exposed to the stream of water between the vortices. As the air flow rate was increased the pressure within the pair of cavities increased and the aerated vortex cores grew larger in size.

With further reduction in the value of cavitation parameter, the vortex cores were seen to coalesce and the wall of water between the vortices degenerated into a thin septum growing in thickness as it was convected downstream, finally striking the fairing which surrounded the model support strut. This septum is difficult to observe visually in the Free-Surface Tunnel because it must be seen through the cavity walls. Because of background tunnel turbulence, the cavity wall is not perfectly smooth but shows, instead, small waves and ripples. The resulting optical distortion makes

it relatively difficult to see details within the cavity. To help increase the contrast between the septum and the ambient stream and, incidently, to obtain qualitative information about the flow in the vicinity of the cavity walls, a jet of dye was directed against the bubble wall about 3/4 of an inch behind the model tip and about 1/8 of an inch above the point where the bubble springs free from the wetted lower surface. (Model 1C in Figure 3). This dye streak can be seen in the sketch of Figure 4 and in the photograph of Figure 5. After striking the cavity wall, the dye is carried along a stream line over the "top" of one of the cavity lobes into the septum. Observation of the dye streak in the septum is difficult because it must be viewed through the curved and "wrinkled" cavity wall and because the dye has begun to diffuse.

That the septum is not peculiar to this particular model or to any particular model orientation can best be seen by inspection of Figures 6 and 7. Figure 6 shows the 15 degree delta wing mounted in an inverted position within the tunnel working section, while Figure 7 presents models of various apex angles within the range of 10 degrees to 90 degrees as well as V-bottom and the 15 degree diamond plan form models. The appearance of the septum at moderate angles of attack is substantially the same for all of these models.

The side views of the cavity, as well as the sketch of Figure 4 show an interesting feature of the flow. Tufts which were attached to the bottom of the model and which were too long, slipped over the sharp edge and streamed along the cavity wall, thereby indicating the direction of flow in this region. Although careful angle measurements were not undertaken, inspection of the photographs shows that the flow angle is not sensitive to the cavitation number nor to the presence of the free surface (Figure 8). For the 15 degree apex angle delta wing, these tufts make an angle with the undisturbed stream direction approximately as shown in Figure 4, and are independent of the model angle of attack for angles from 21 degrees to 30 degrees.

When seen from below, the tuft studies (Figure 9) show the relative insensitivity of the flow direction, along the model surface, to cavitation number and to model submergence. Since it was not possible to obtain

high cavitation numbers at low submergences or low cavitation numbers at deep submergences, the spaces where the corresponding photographs belong have been left blank. It should be noted that the photographs in Figure 9 were taken vertically, from below the water tunnel. To eliminate the apparent foreshortening due to the 30 degree angle of attack of the model, the pictures were rectified during enlargement to produce a true view of the plane of the model.

Effect of Model Submergence and Specification of Cavitation Number

Since the early experiments of Reichardt[8] it has been recognized that the hydrodynamic forces and moments acting on a body which produces large open cavities in its wake are the same whether that cavity is filled with water vapor or with air, so long as the cavitation parameter is given in terms of the measured cavity pressure. The cavitation parameter is usually expressed in the form

$$K = \frac{p_o - p_k}{\frac{1}{2}\rho V_o^2}$$

When the cavity pressure and tunnel velocity are measured by means of water-filled manometers it is convenient to express the cavitation number as

$$K = \frac{h_o - h_k}{\frac{V^2}{2g}}$$

where h_k is the reading of a water-filled manometer (in feet) measuring the cavity pressure, and h_o is the pressure head (in feet) far ahead of the model in the undisturbed flow. Since only the difference $h_o - h_k$ is important, both pressures may conveniently be measured with respect to the atmosphere, and $h_o = Y_o$ is merely the model submergence in feet. The denominator equals the reading of a water-filled manometer, referred to the moving water surface in the working section, and connected to a tap located at any convenient point upstream of the tunnel nozzle.

For air-supported cavities at velocities less than 25 fps, the value of

h_k is usually within a few tenths of a foot of atmospheric pressure. Under these conditions the specification of the cavitation number becomes ambiguous since the value of h_o will necessarily vary over a wide range for relatively long models inclined to the flow. If the notion of a "local" cavitation number

$$K_\ell = \frac{Y_o - h_k}{\frac{V^2}{2g}}$$

is adopted to examine the importance of the difference in static pressure at the extreme ends of the model, and if Reichardt's well known formula $C_D = C_{D_o}(1 + K)$ for drag applies to elementary strips at varying depths, then it follows that the normal forces acting on the cavity-producing body can be regarded as being made up of three terms

$$C_{D_o}\frac{\rho}{2} V^2 A - C_{D_o}^{\gamma} h_k A + C_{D_o}^{\gamma}\int_{Y_1}^{Y_2} 2zY\,dY$$

where only the last term depends on submergence and is equal to $C_{D_o} A Y^*$.

For the conditions of velocity and pressure examined during these tests "local" cavitation numbers are actually negative at the tip of the model.

Using similar procedures, it can be shown that the moment coefficient or the center of pressure location should also be corrected for the effect of difference in depth along the model, but these can be neglected since in the worst case (in which the model tip just breaks through the water surface) the error introduced by assuming that the "hydrostatic" forces act at the centroid is less than the experimental scatter.

Lift and drag measurements taken at an angle of attack of 21 degrees, show no significant variation even when the model broaches the free surface, and as much as one quarter area of the model lies above the undisturbed water surface. Under these conditions the septum no longer exists; instead the cavity bubble exhibits a longitudinal gap which starts at the model tip and increases in width downstream, creating a V-shaped opening which connects the bubble with the outside air. If the force coefficients are

based on the plan form area of the model below the undisturbed water surface, these constant force values mean that the lift and drag coefficients increase slightly when the model pierces the free surface.

Force and Pressure Measurements

The results of the force measurements made on the superventilated delta wing models are presented in Figures 10 through 15 for models with increasing apex angle. In these figures lift and drag coefficients are plotted as a function of model cavitation number, K, as is the position of the center of pressure $\bar{x}$. The force coefficients and cavitation (or ventilation) number have been defined in the usual way (see list of symbols on pages i and ii).

Figure 11, which presents the results of the measurements performed on the 15 degree delta wing, presents data taken over a greater range of operation parameters than has been done for the other models since this model had been singled out for exploration of the effect of variations in submergence, model scale, etc. The results for angles of attack less than 21 degrees and those for cavitation numbers less than 0.05 were obtained by running the model nearer the free surface than the 0.65 ft. value used for the main test sequence. As pointed out previously, in some cases the model tip was permitted to broach the water surface.

The effect of apex angle on the force and moment coefficients at a constant value of cavitation number and angle of attack is presented in the cross plot shown in Figure 16.

Some indication of the effect of model dead rise and plan form, as well as of deviations from standard orientation and configuration, are shown in Figure 17 for models with a nominal apex angle of 15 degrees and at a 30 degree angle of attack.

A comparison of Figure 17 with Figure 11 shows that inverting the model in the tunnel had no significant effect on the measured force coefficients or on the position of the center of pressure. Likewise, the effect of blunting the model, which had been done in an attempt to secure better cavity bubble formation at the lower angles of attack had no significant effect on the measured coefficients.

Running the model backwards so that the 15 degree apex trailed

downstream resulted in lift and drag coefficients very close to those obtained for the orthodox configuration. The center of pressure, measured in all cases from the trailing edge of the model shows a more pronounced shift upstream from the centroid of the plan form and the re-entrant jet or septum is not formed when the model is in this attitude. Instead, the upper surface of the cavity bubble soon is flat in transverse section where it leaves the leading edge of the model and soon becomes more concave (downward) as the section is taken farther downstream.

The diamond-shaped model Number 8 and the 90 degree V-bottom Model 3A, were tested only to explore, in a preliminary way, the effect of the change in model plan form and dead rise on the measured force coefficients and on the observed flow geometry.

The pressure distributions of Figures 18 and 19 supplement the information provided by the force measurements and provides better insight into the effect of change of angle of attack and cavitation number on the 15 degree model. The pressure coefficient as used here is referred to the cavity pressure p_k instead of the free stream static pressure p_o, as is customarily employed for fully-wetted flows. Using this notation the stagnation pressure is equal to 1 + K and the pressure coefficient anywhere within the cavity bubble is taken as zero. The plan form of the model is included in these figures to show the approximate location of the pressure taps and to define the distance coordinates used in the pressure distribution plots. From this drawing it can be seen that the pressure taps are located along selected rays drawn through the tip of the model. In the left hand curves both the longitudinal center line pressure distribution and the individual transverse section pressure distributions (shown rotated into the plane of the paper) give a graphical representation of the pressure forces which act normal to the model. For clarity of presentation, pressure readings from only the left hand side of the model have been included in these transverse views, and the transverse tap position, although drawn to the same scale as the longitudinal position, has not been identified for each of the sections. The representation on the right hand side of the figures shows the pressure coefficient at each of the transverse stations drawn superimposed and normalized to the value of pressure coefficient at the

centerline. Within the accuracy of the pressure measurements the transverse pressure distributions are not affected by the longitudinal position of the station along the model, nor is the nature of the pressure distribution significantly affected by changes in the cavitation number or angle of attack of the model over the range of values of these variables shown in the figures.

When the angle of attack of the model was reduced to 15 degrees, and the model was permitted to approach the water surface in order to secure low cavitation numbers, an interesting change in the pressure distribution was observed:

(1) Because of an apparent tunnel flow asymmetry near the surface, the pressure distribution was not symmetrical with respect to the model centerline. (Compare tufts in Figure 9.)

(2) A pressure distribution, more nearly in agreement with those in Reference 2 were obtained, that is, the pressure coefficient increased, rather than decreased, for rays outboard of the model centerline.

These latter distributions have not been included since the effect of the flow asymmetry may be producing non-representative values.

ACKNOWLEDGMENTS

This report represents the combined efforts of many individuals: Mr. Murphy Lum, who carried out most of the force and pressure measurements; Mrs. Laura Gaard, who performed the calculations and prepared the curves; Mr. Carl Eastvedt, who took the photographs; and Mr. George Lundgren, who fabricated the models and model attachments. The helpful suggestions of Professors Acosta and Wu were instrumental in determining the scope and direction of the experiments.

REFERENCES

1. Jones, R. T., "Properties of Low-Aspect Ratio Pointed Wings at Speeds Below and Above the Speed of Sound", Technical Note No. 1032, Langley Memorial Aeronautical Laboratory, March 1946.

2. Lee, G. H., "Note on the Flow Around Delta Wings With Sharp Leading Edges", Aeronautical Research Council R and M No. 3070, 1958.

3. Tulin, M. P., "Supercavitating Flow Past Slender Wings", Journal of Ship Research, Vol. 3, No. 3, p. 17, 1959.

4. Reichardt, H. and Sattler, W., "Three-Component Measurements on Delta Wings With Cavitation", Max-Planck Institut fuer Stroemungsforschung, Goettingen, July 1962.

5. Knapp, R. T., Levy, J., O'Neill, J. P., and Brown, F. B., "The Hydrodynamics Laboratory of the California Institute of Technology", Trans. ASME, July 1948.

6. Kiceniuk, Taras, "An Experimental Study of the Hydrodynamic Forces Acting on a Family of Cavity-Producing Conical Bodies of Revolution Inclined to the Flow", California Institute of Technology, Report No. E 12.17, June 1954.

7. Wu, T. Y. and Cumberbatch, E., "Cavity Flow Past a Slender Pointed Hydrofoil", Vol. II Journal of Fluid Mechanics, pp. 187-208, 1961.

8. Reichardt, H., "The Laws of Cavitation Bubbles at Axially Symmetrical Bodies in a Flow", R and T No. 766, Ministry of Aircraft Production, August 15, 1946.

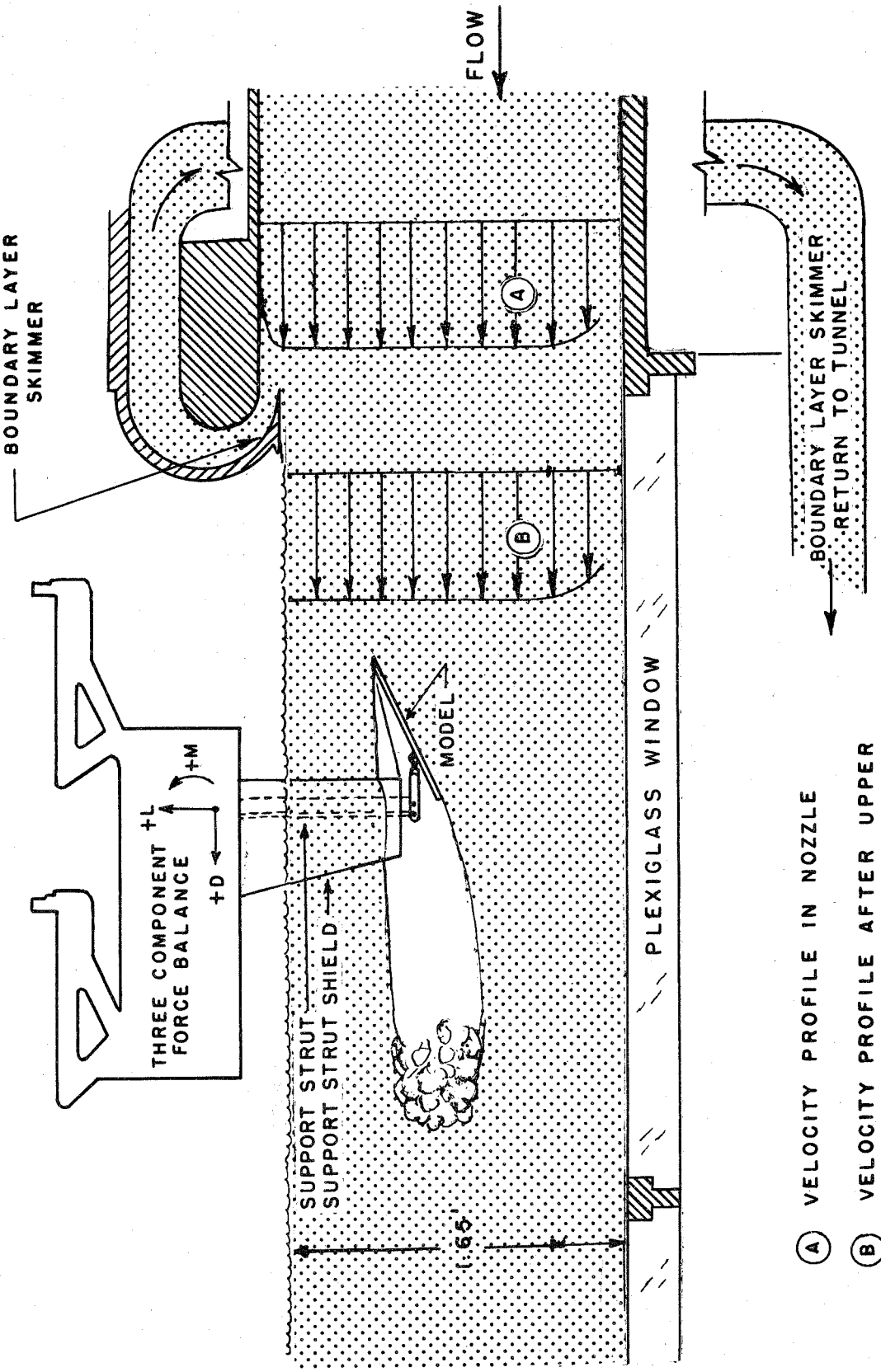

Fig. 1 - Diagram of the Free-Surface Water Tunnel Working Section

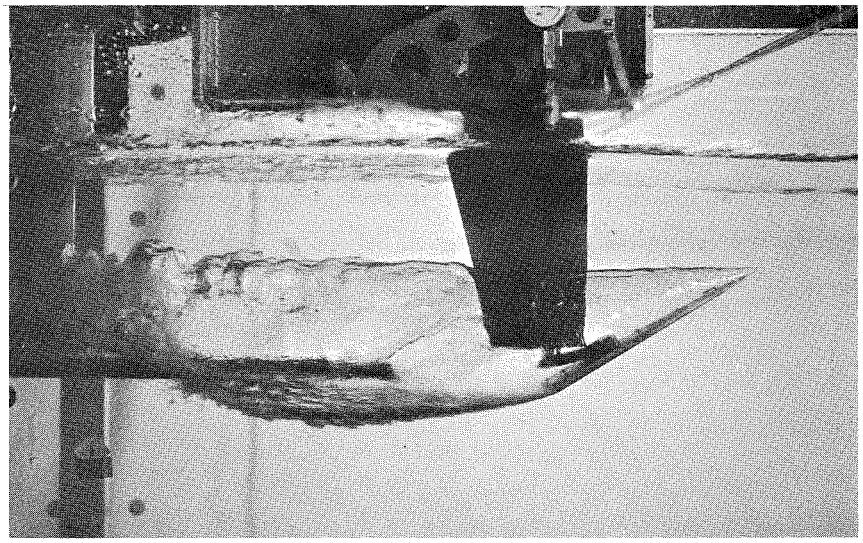

(a) $\alpha = 30^{o}$ K = .120 V = 14 fps

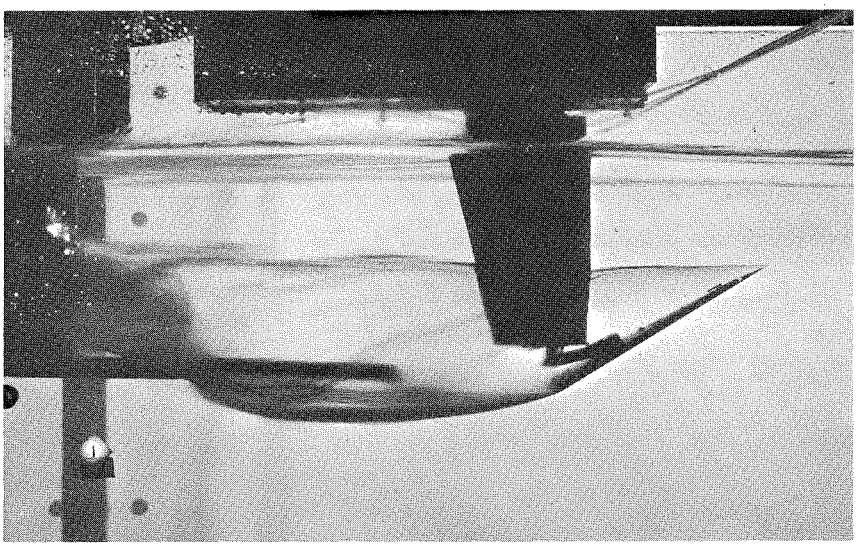

(b) $\alpha = 30^{o}$ K = .121 V = 14 fps

Fig. 2 - 15^{o} Delta Wing Supported from the Three-Component Force Balance in the Working Section of the Free-Surface Water Tunnel. Electronic Flash was Used in (a) Above; Time Exposure in (b).

(a)
Model 1 C

Apex Angle - 15°
Length - .693 ft
Area - .064 ft^2

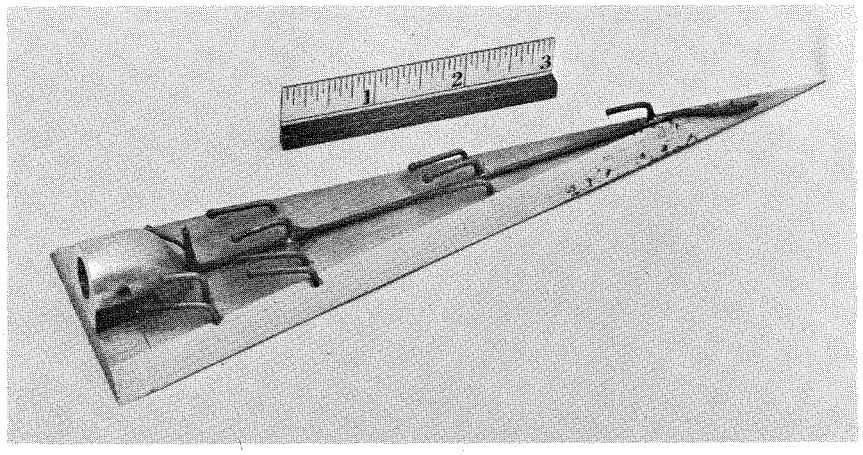

(b)
Model 2 C

Apex Angle - 15°
Length - .653 ft
Area - .058 ft^2

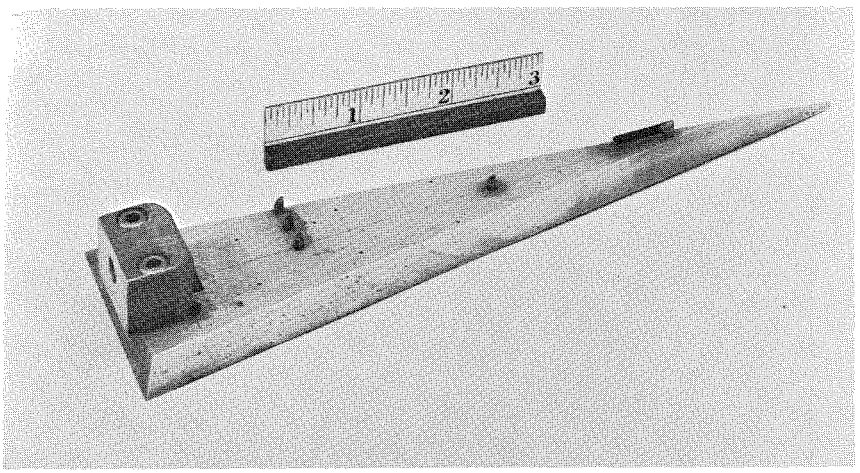

(c)
Model 3A

Apex Angle - 15°
Length - .600 ft
Area - .048 ft^2

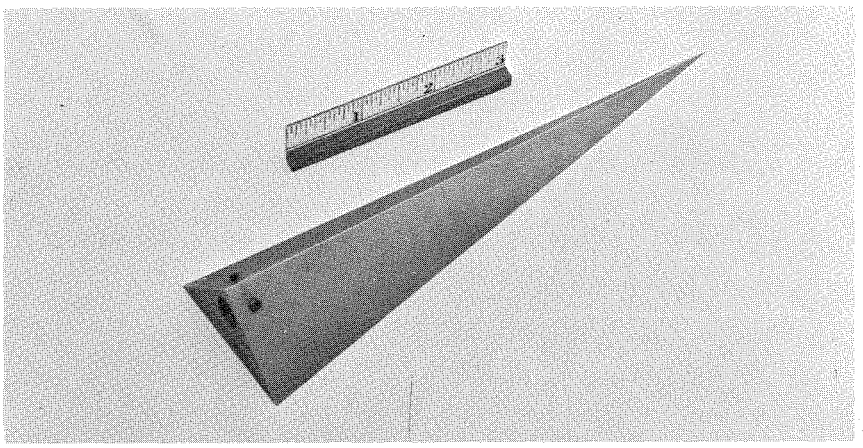

Fig. 3 - Delta Wing Models

(d)
Model 4

Apex Angle - 45°
Length - .375 ft
Area - .058 ft^2

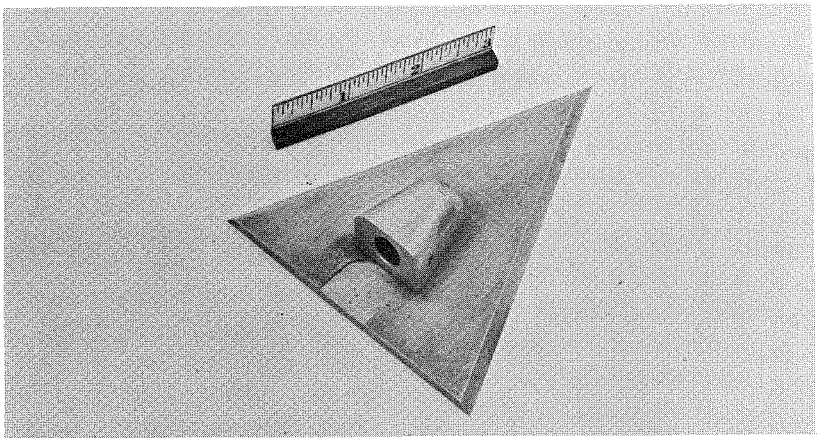

(e)
Model 5

Apex Angle - 90°
Length - .250 ft
Area - .063 ft^2

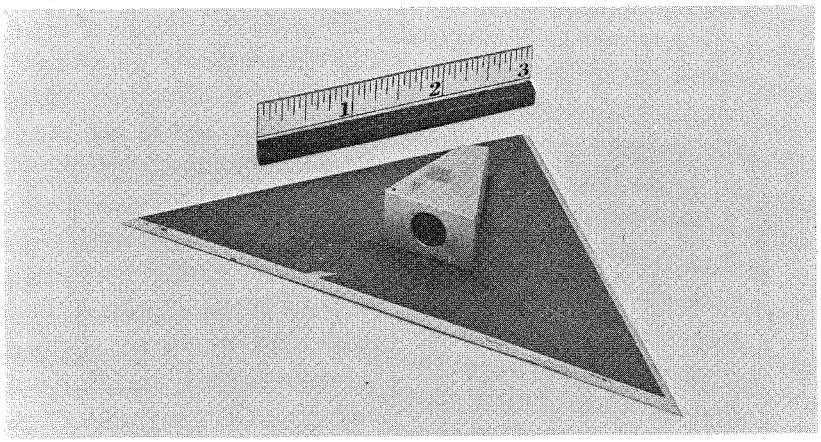

(f)
Model 6

Apex Angle - 60°
Length - .333 ft
Area - .064 ft^2

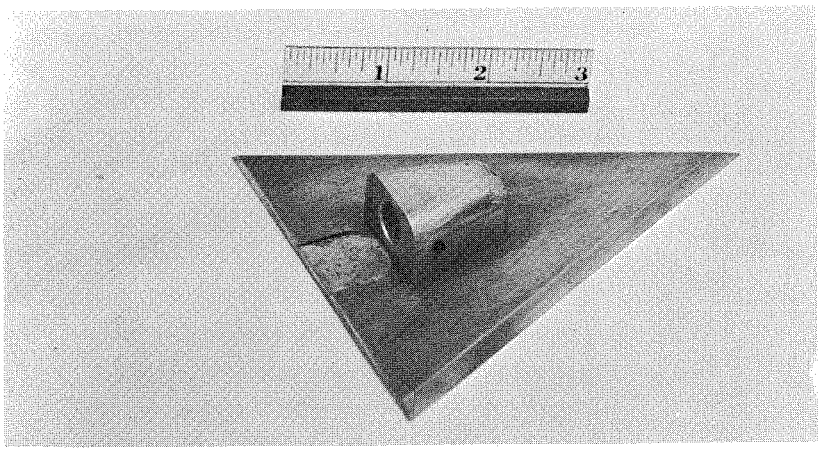

Fig. 3 - (Continued) Delta Wing Models

(g)
Model 7

Apex Angle - 30°
Length - .458 ft
Area - .056 ft^2

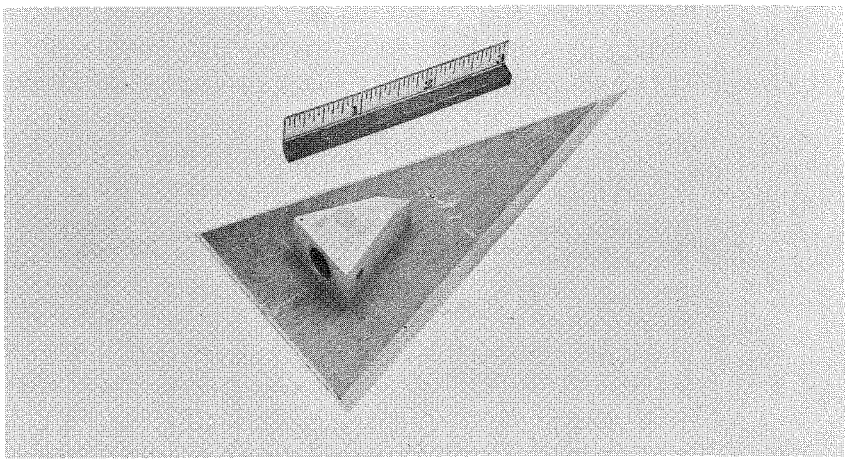

(h)
Model 8

Apex Angle - 15°
Length - .906 ft
Area - .054 ft^2

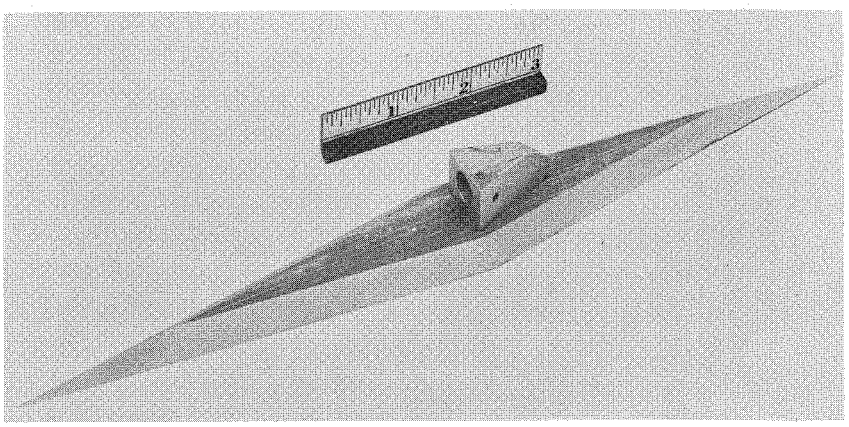

(i)
Model 9

Apex Angle - 10°
Length - .828 ft
Area - .060 ft^2

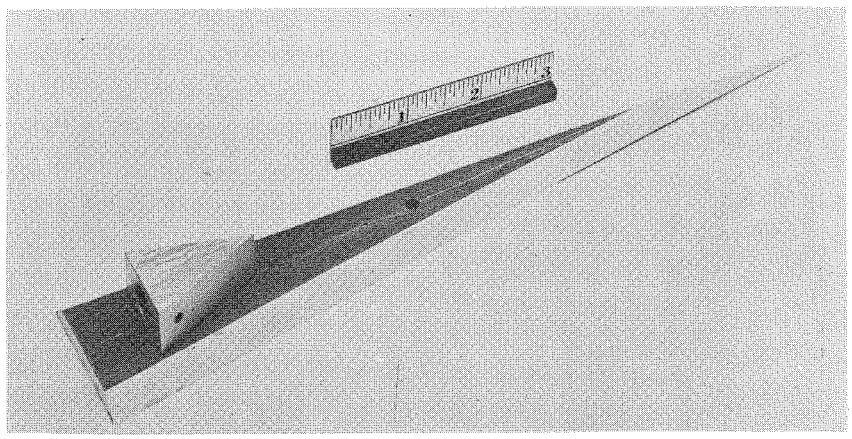

Fig. 3 -(Continued) Delta Wing Models

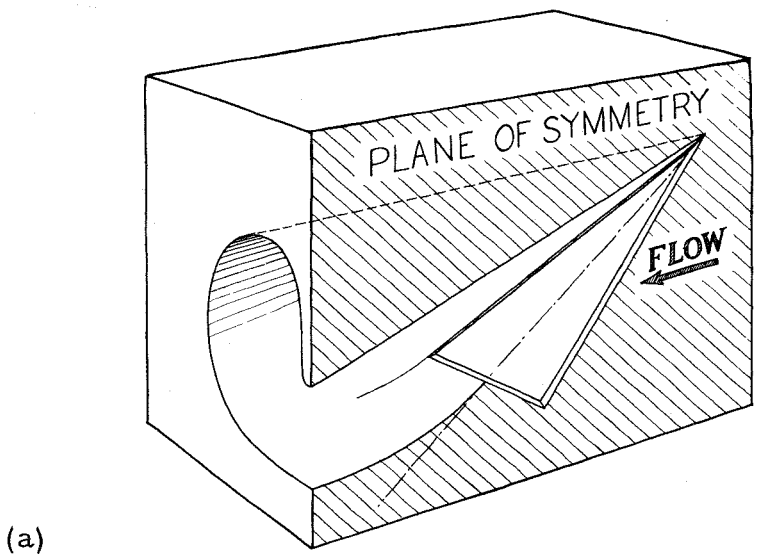

(a)

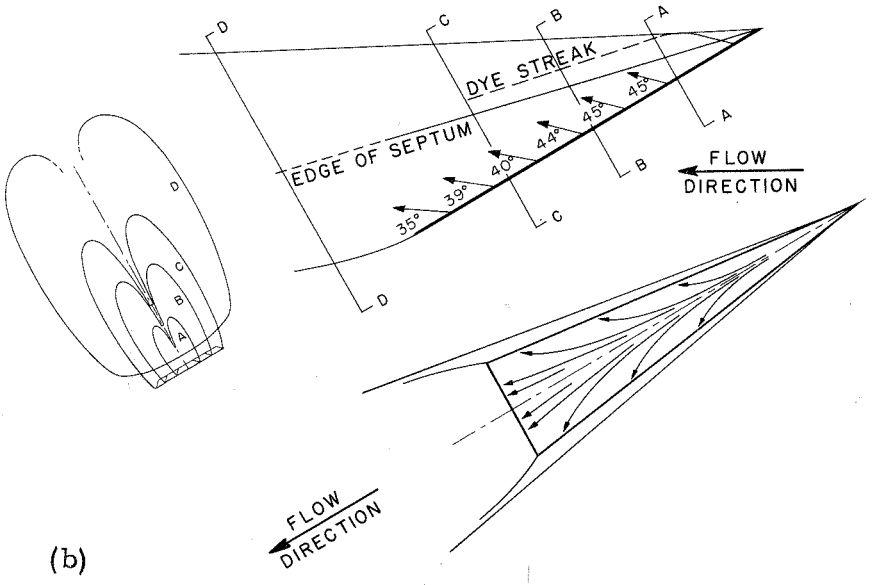

(b)

Fig. 4 - Diagrammatic Sketch of Superventilated Flow Past a 15° Delta Wing at a Low Cavitation Number and an Angle of Attack of 30°.

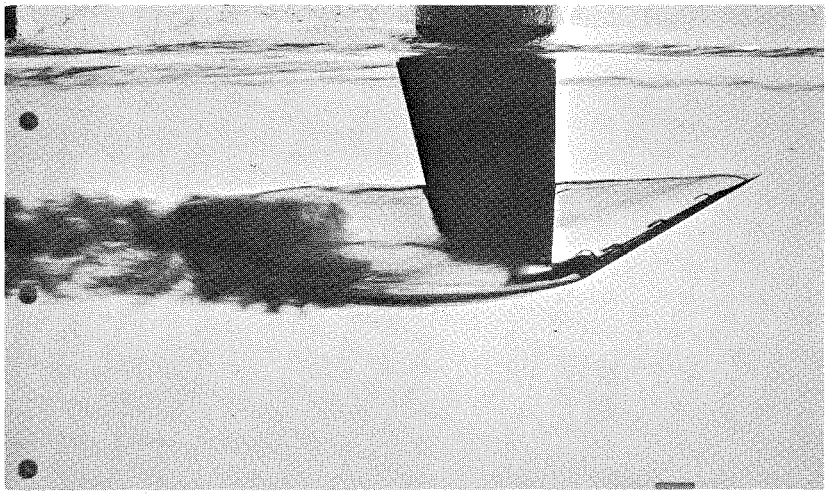

Fig. 5 - 15° Delta Wing Showing Injected Dye Streak and Septum. $\alpha = 30^{\circ}$, V = 14.7 fps, K = .13.

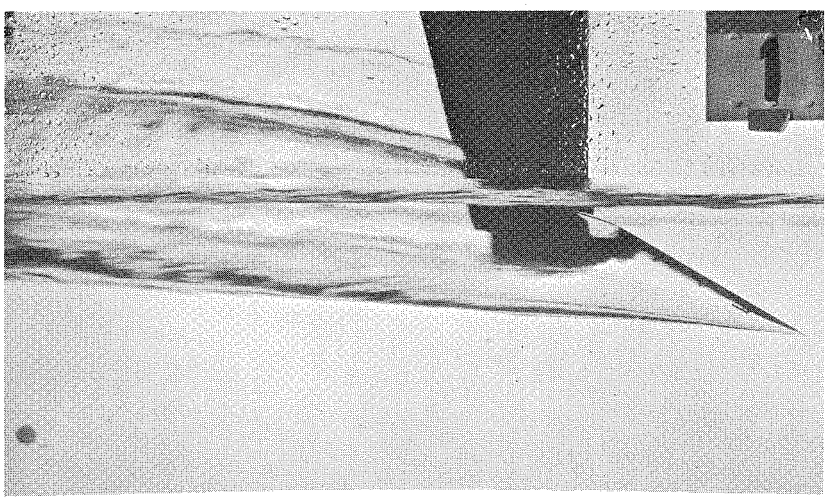

Fig. 6 - 15° Delta Wing Inverted in Tunnel. $\alpha = -30^{\circ}$, V = 16 fps.

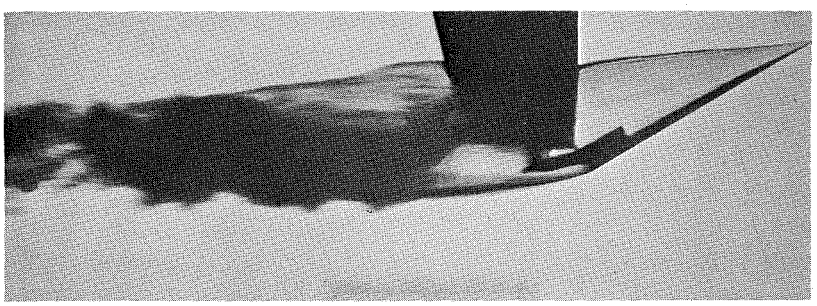

(a) $\gamma = 10^{o}$ $\alpha = 30^{o}$

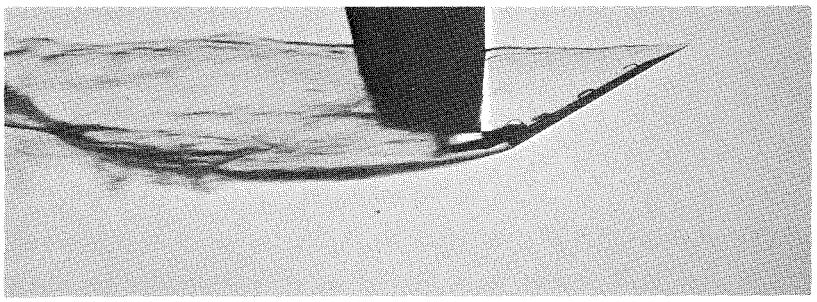

(b) $\gamma = 15^{o}$ $\alpha = 30^{o}$

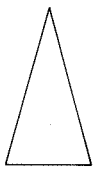

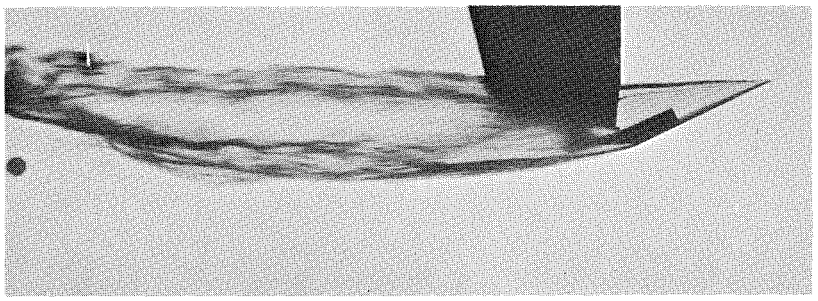

(c) $\gamma = 30^{o}$ $\alpha = 30^{o}$

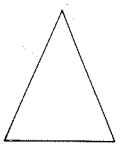

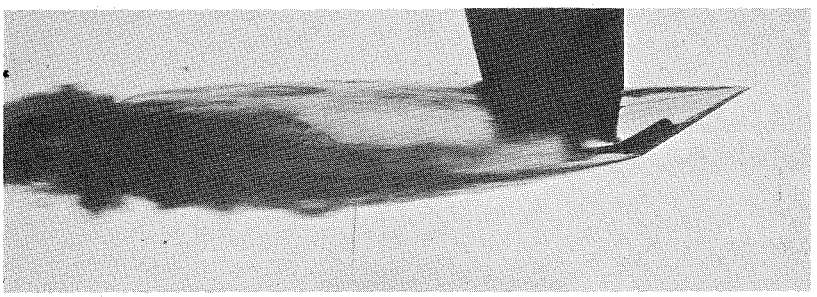

(d) $\gamma = 45^{o}$ $\alpha = 30^{o}$

Fig. 7 - Superventilating Delta Wings of Various Apex Angles at Moderate Angle of Attack.

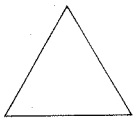

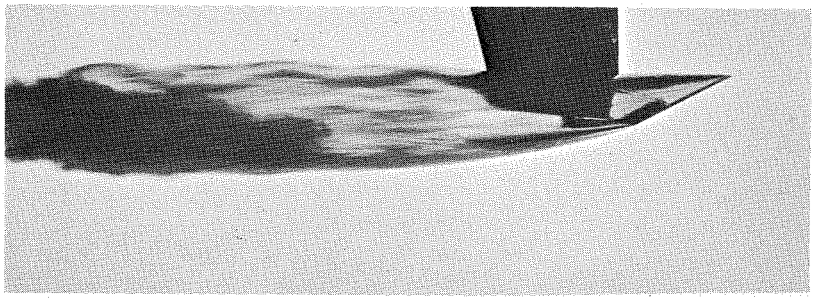

(e) $\gamma = 60^{\circ}$ $\alpha = 30^{\circ}$

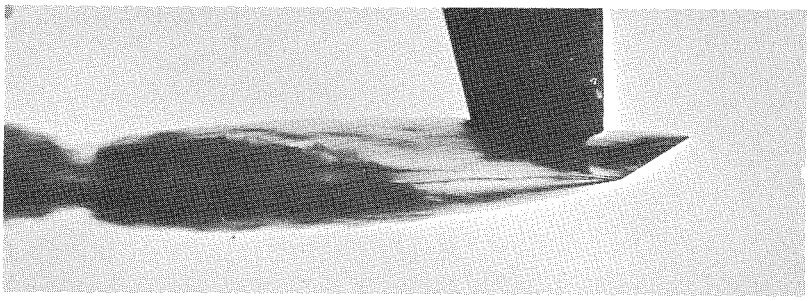

(f) $\gamma = 90^{\circ}$ $\alpha = 30^{\circ}$

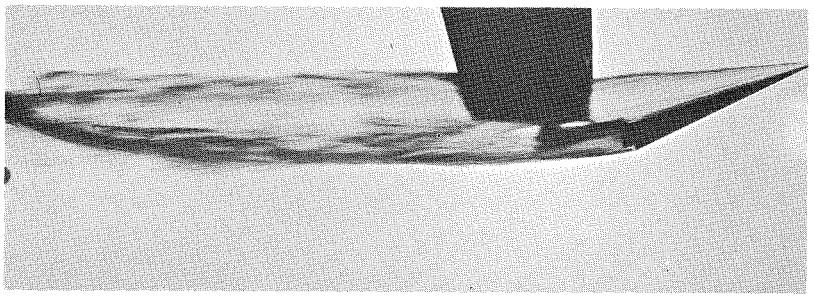

(g) $\gamma = 15^{\circ}$ (90° V-Bottom) $\alpha = 25^{\circ}$

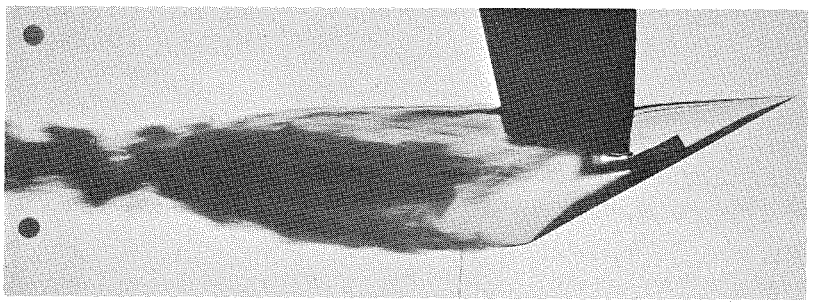

(h) Diamond plan form $\gamma = 15^{\circ}$ $\alpha = 30^{\circ}$

Fig. 7 - (Continued) Superventilating Delta Wings of Various Apex Angles at Moderate Angle of Attack.

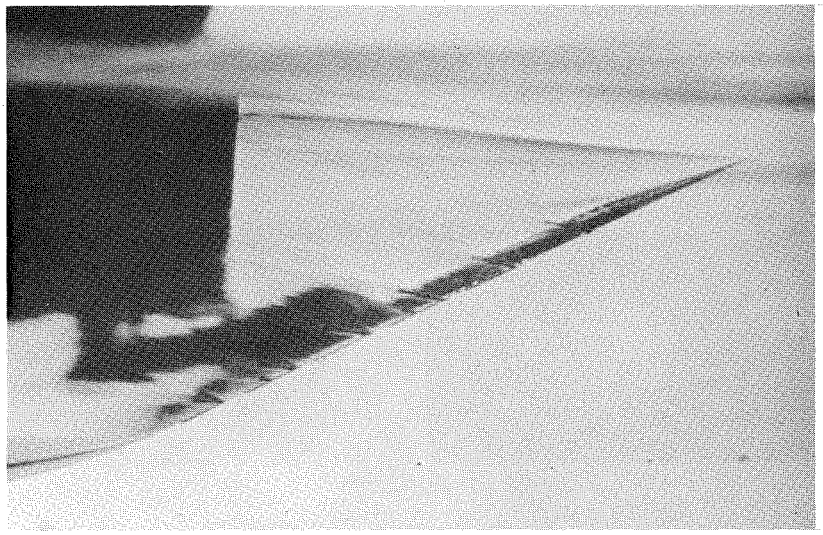

K = .0190

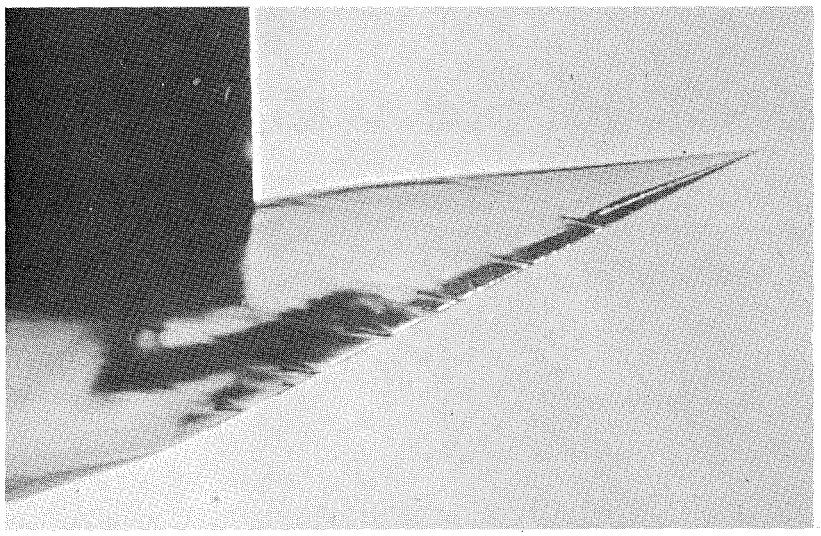

K = .0544

Fig. 8 - Comparison of Flow Direction in Cavity Wall Near Edge of Delta Wing with Apex Angle = 15^{o} and Angle of Attack of 25^{o}. Upper Model is Near Surface (submergence to centroid - .087 ft). Lower Model is at Moderate Depth (submergence to centroid- .57 ft). Model Length is .69 ft.

Submergence, $Y^* = .250$ ft.

Submergence, $Y^* = .650$ ft.

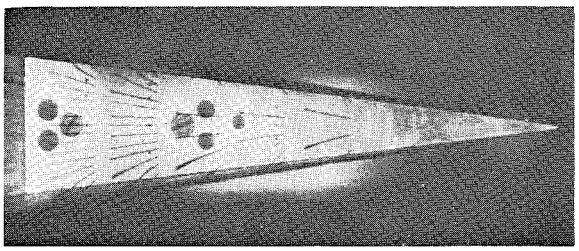

K = .028

Cavitation Number
not Attainable

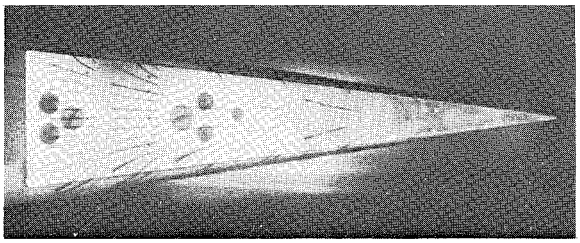

K = .055

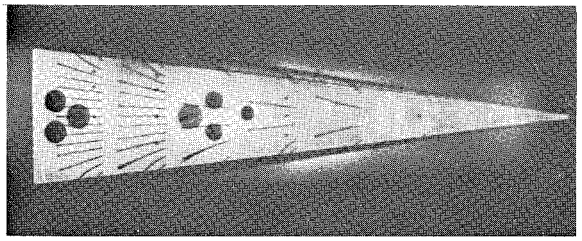

K = .069

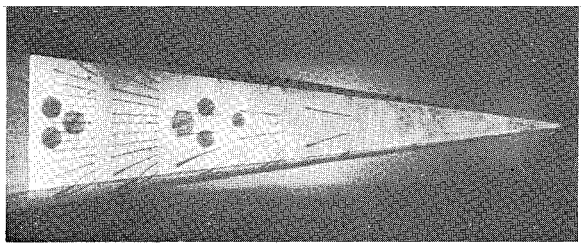

K = .083

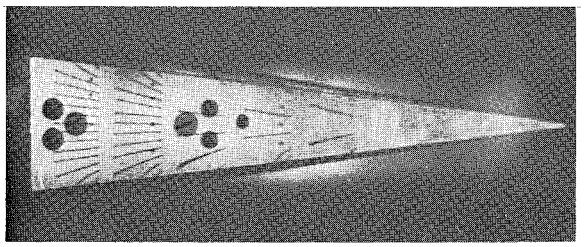

K = .086

Cavitation Number
Not Attainable

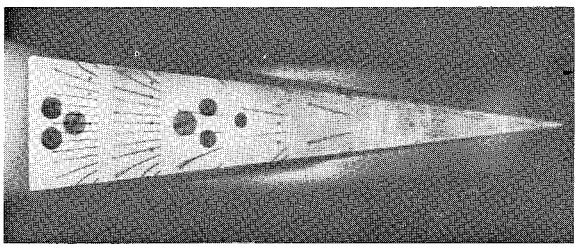

K = .176

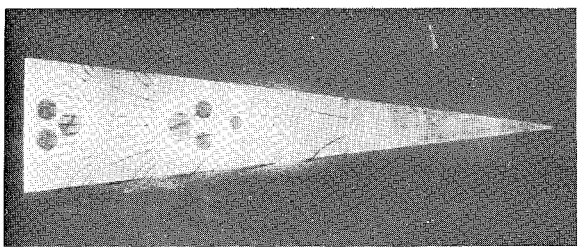

Fully-Wetted

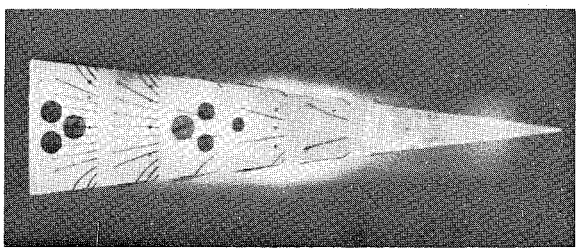

Fully-Wetted

Fig. 9 - Bottom View of Superventilating Delta Wing at Varying Cavitation Numbers and at Two Submergences (.250 feet, left hand column and .650 feet, right hand column). Angle of Attack = 30°, Velocity = 15 fps.

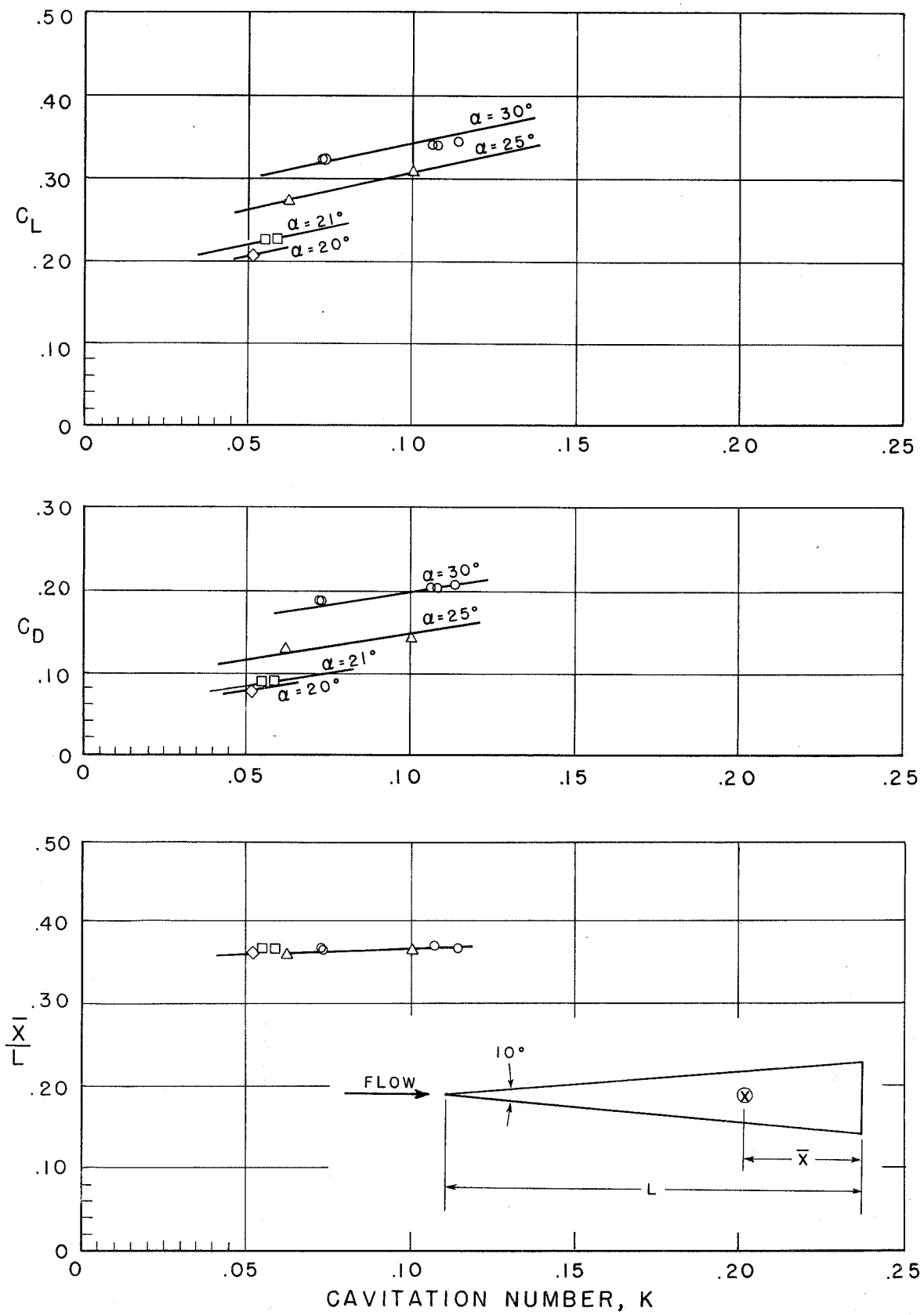

Fig. 10 -Lift, Drag and Center of Pressure Location for a Super-ventilated 10° Delta Wing as a Function of Cavitation Number.

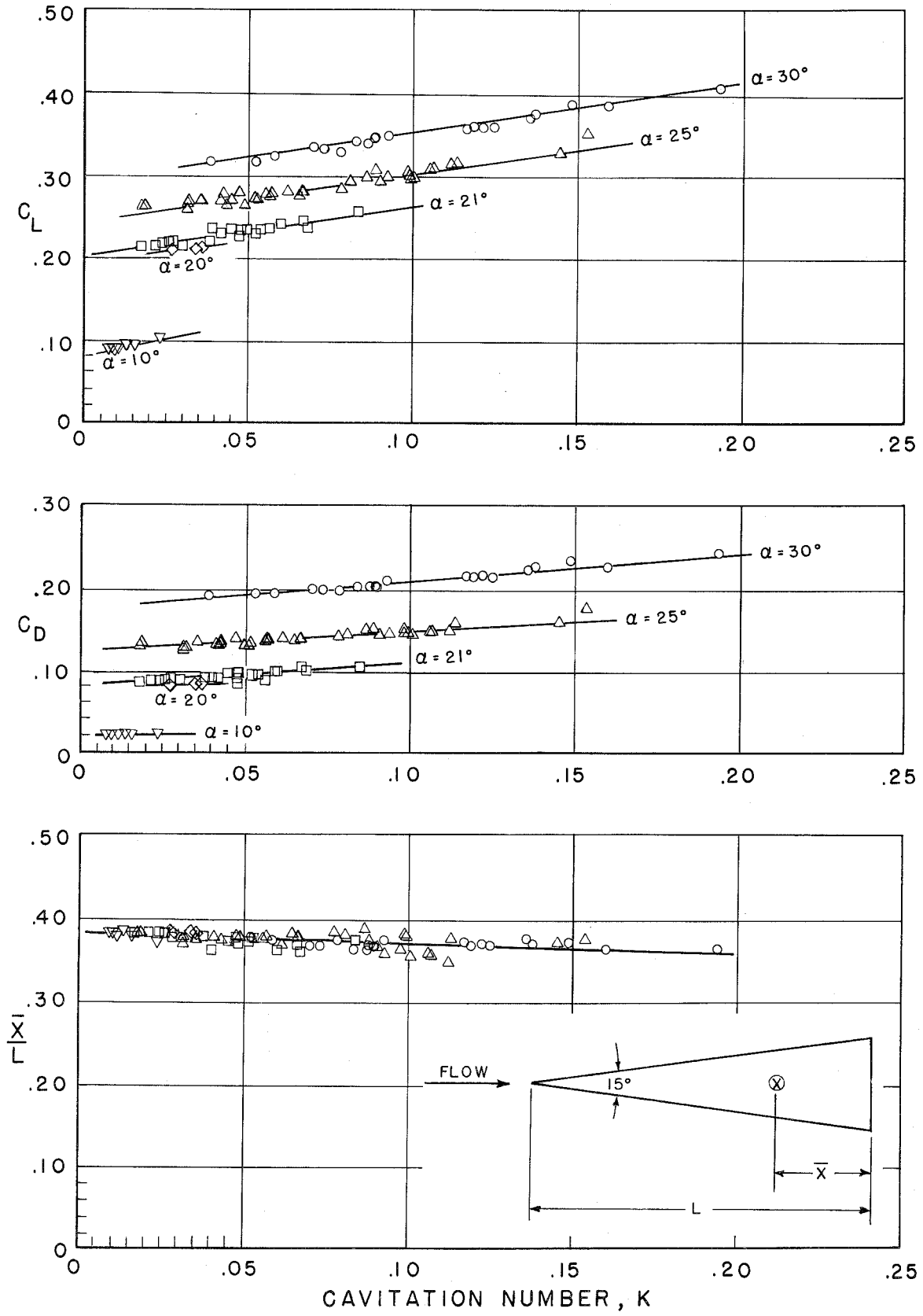

Fig. 11 -Lift, Drag and Center of Pressure Location for a Super-ventilated 15° Delta Wing as a Function of Cavitation Number.

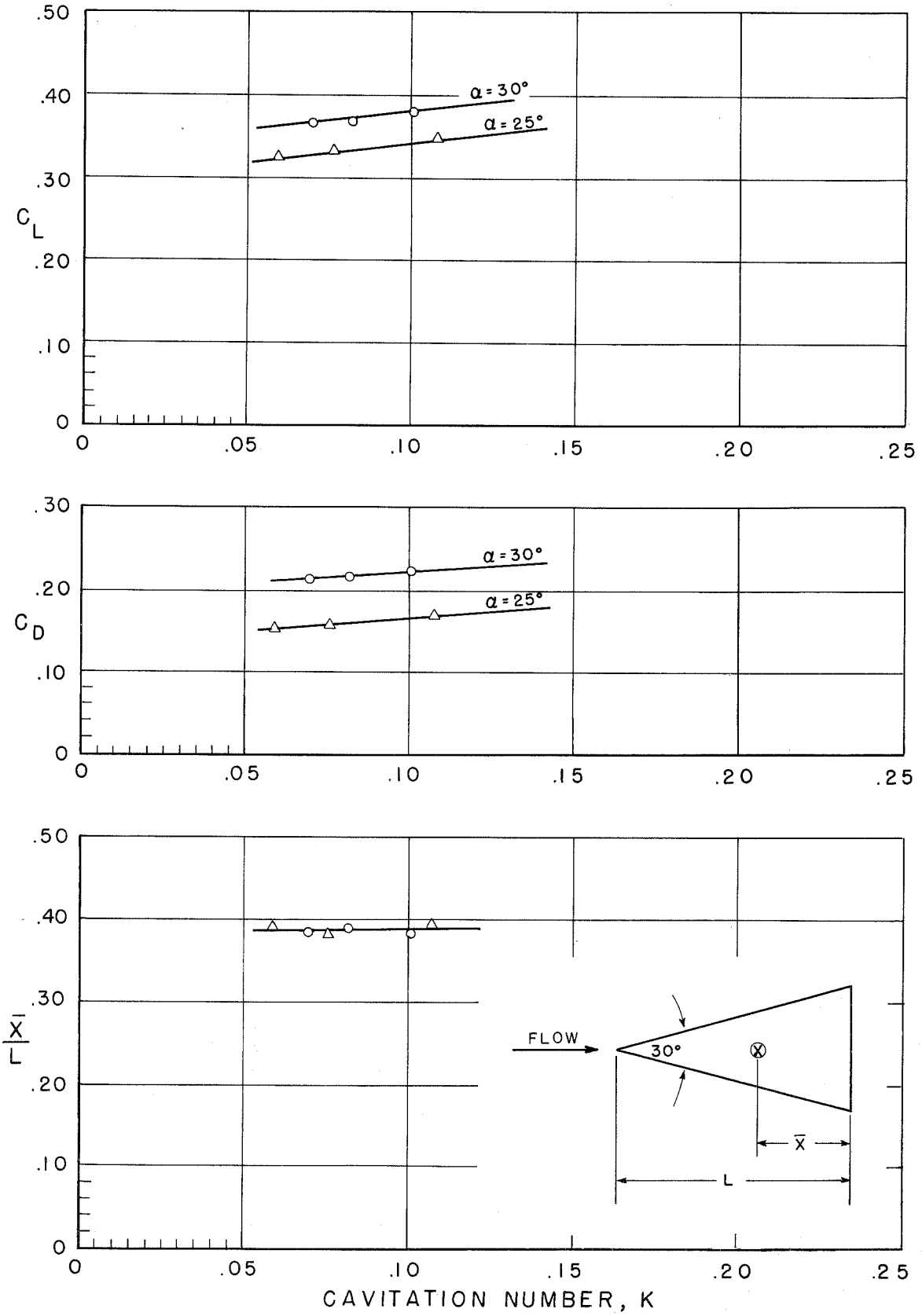

Fig. 12 - Lift, Drag and Center of Pressure Location for a Super-ventilated 30° Delta Wing as a Function of Cavitation Number.

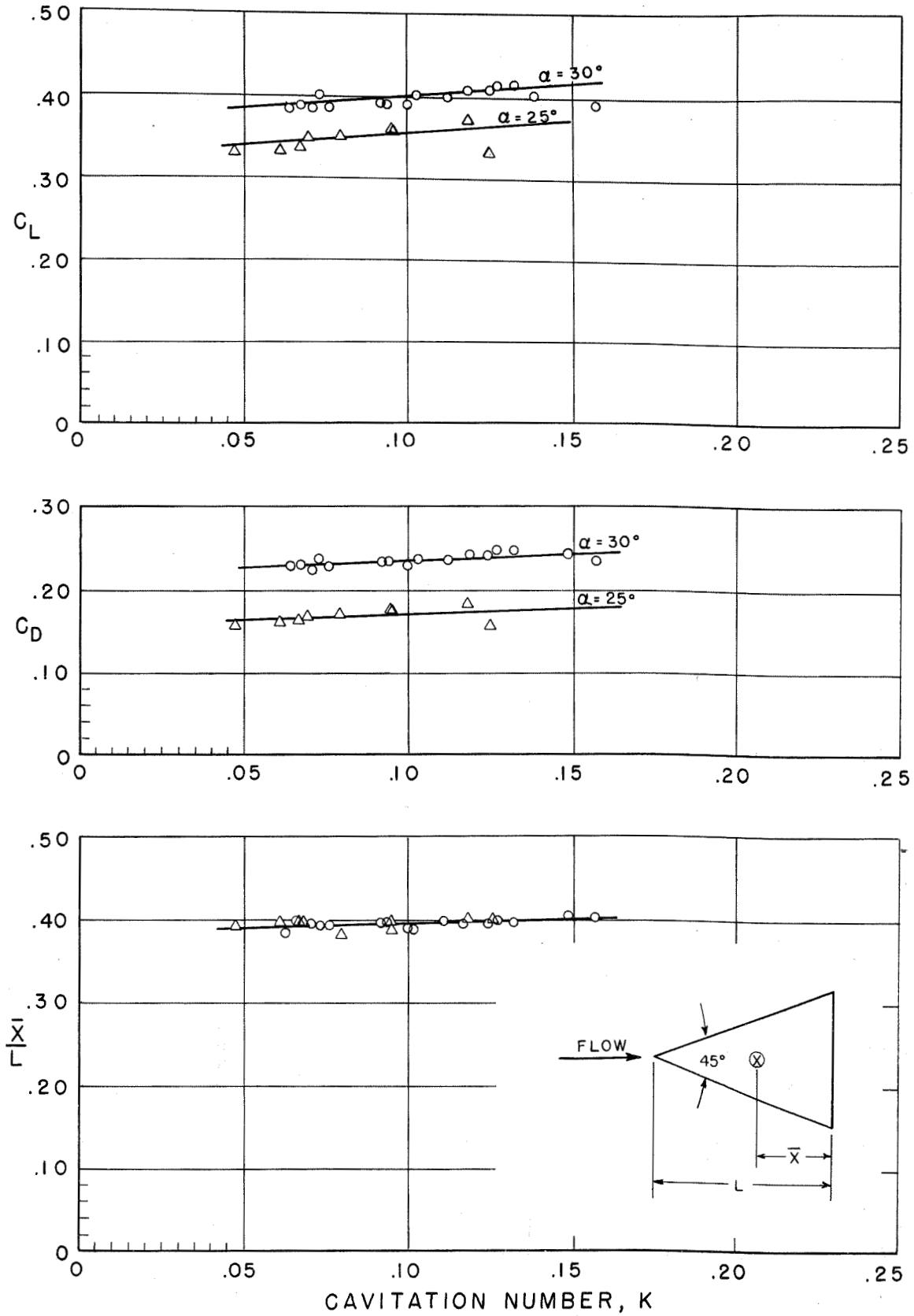

Fig. 13 -Lift, Drag and Center of Pressure Location for a Super-ventilated 45° Delta Wing as a Function of Cavitation Number.

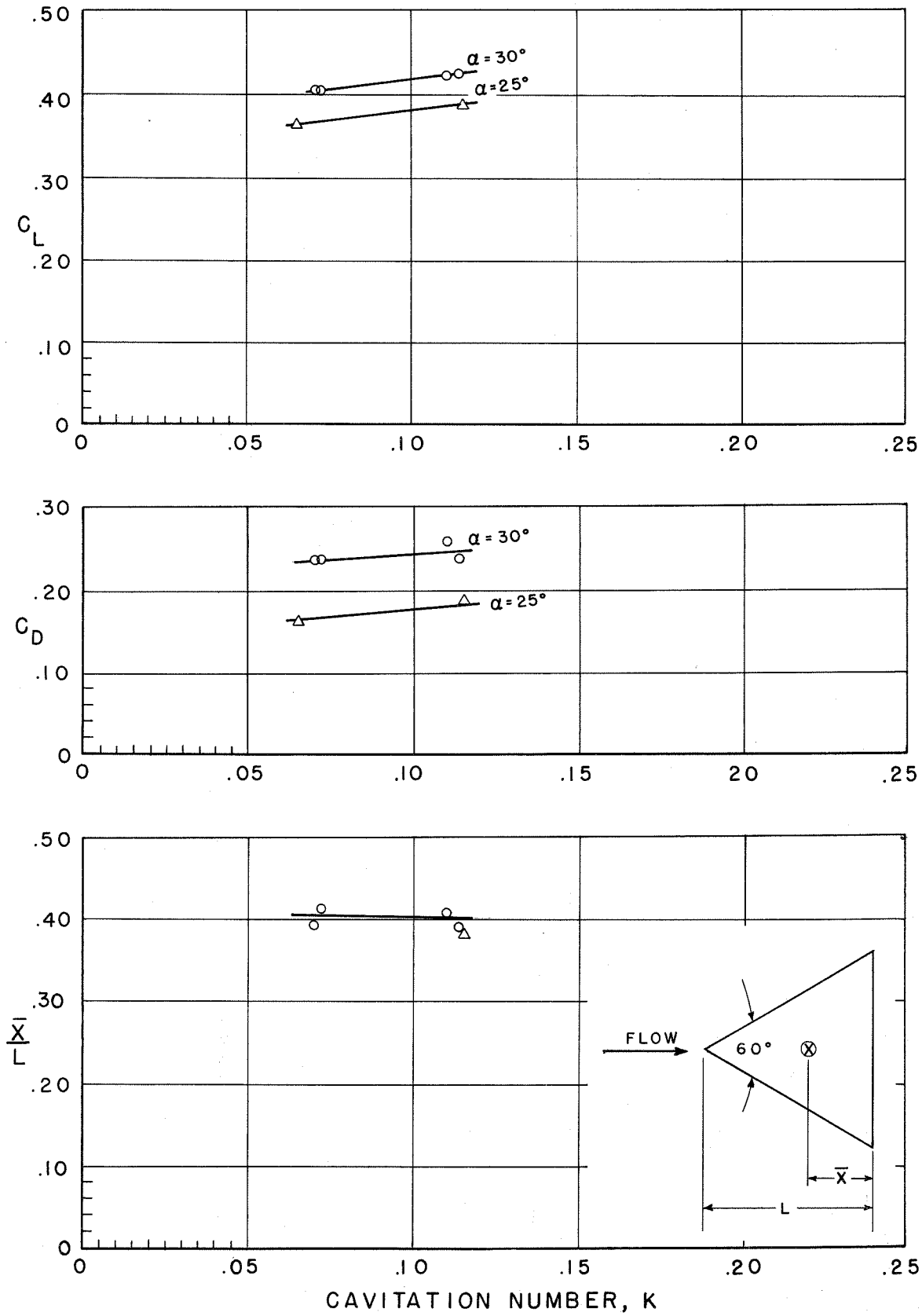

Fig. 14 - Lift, Drag and Center of Pressure Location for a Super-ventilated 60° Delta Wing as a Function of Cavitation Number.

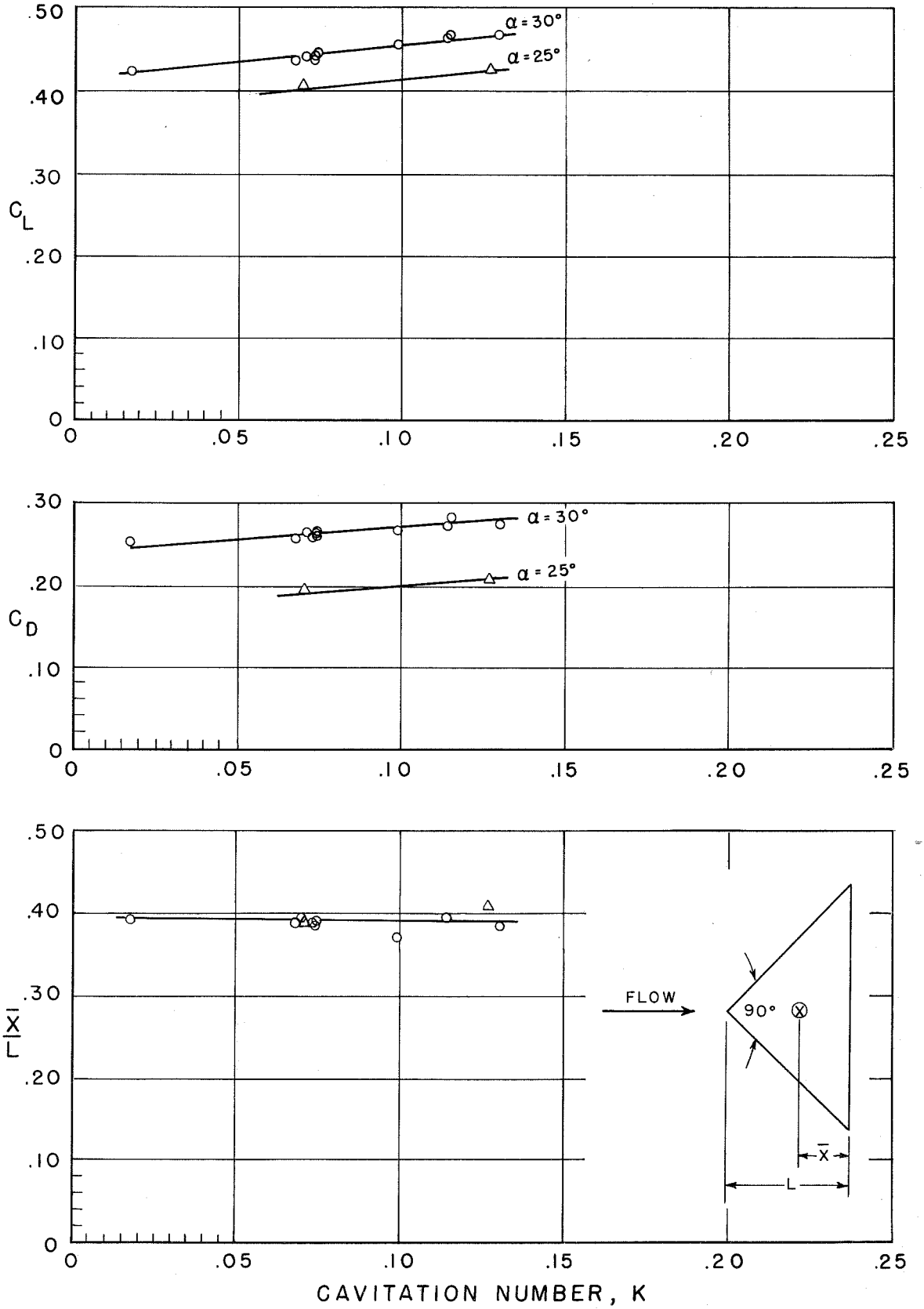

Fig. 15 - Lift, Drag and Center of Pressure Location for a Super-ventilated 90° Delta Wing as a Function of Cavitation Number.

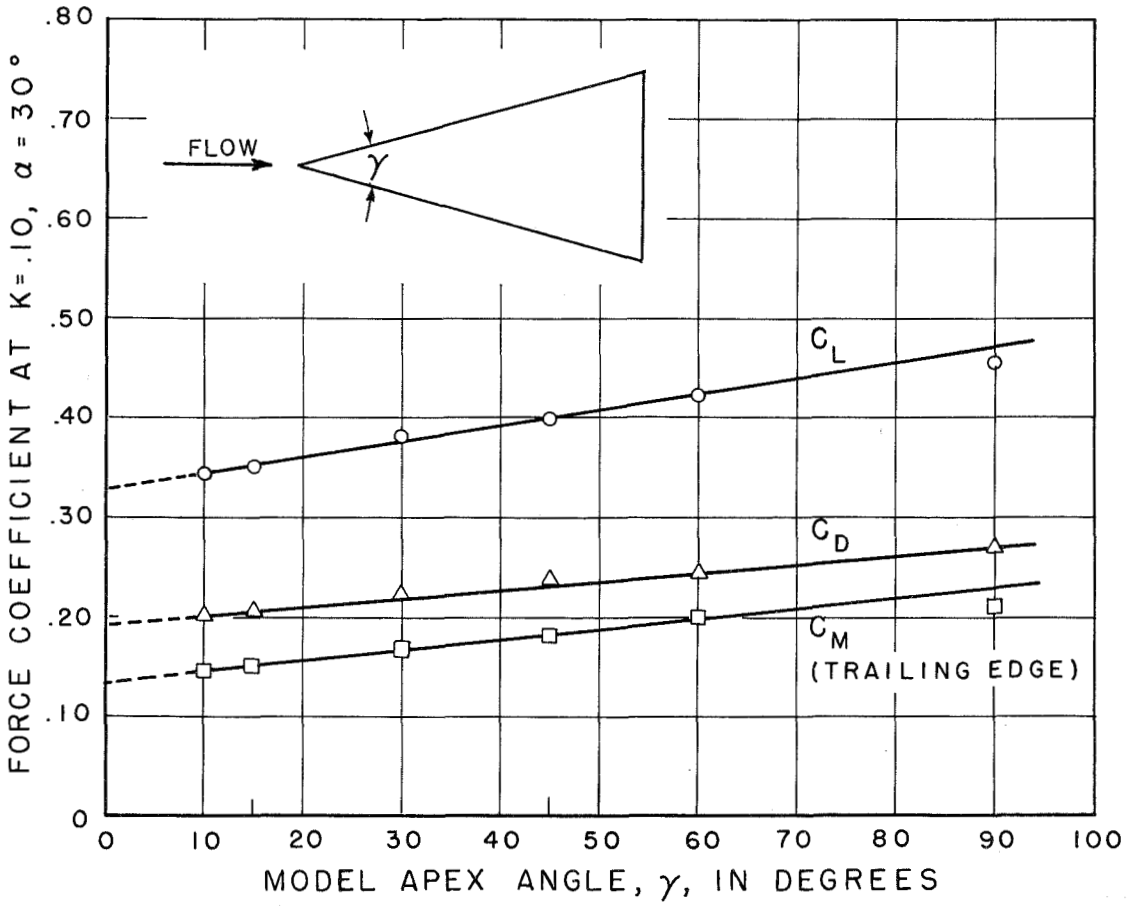

Fig. 16 - Effect of Apex Angle for a Supercavitating Delta Wing at an Angle of Attack of 30° and Cavitation Number of .1.

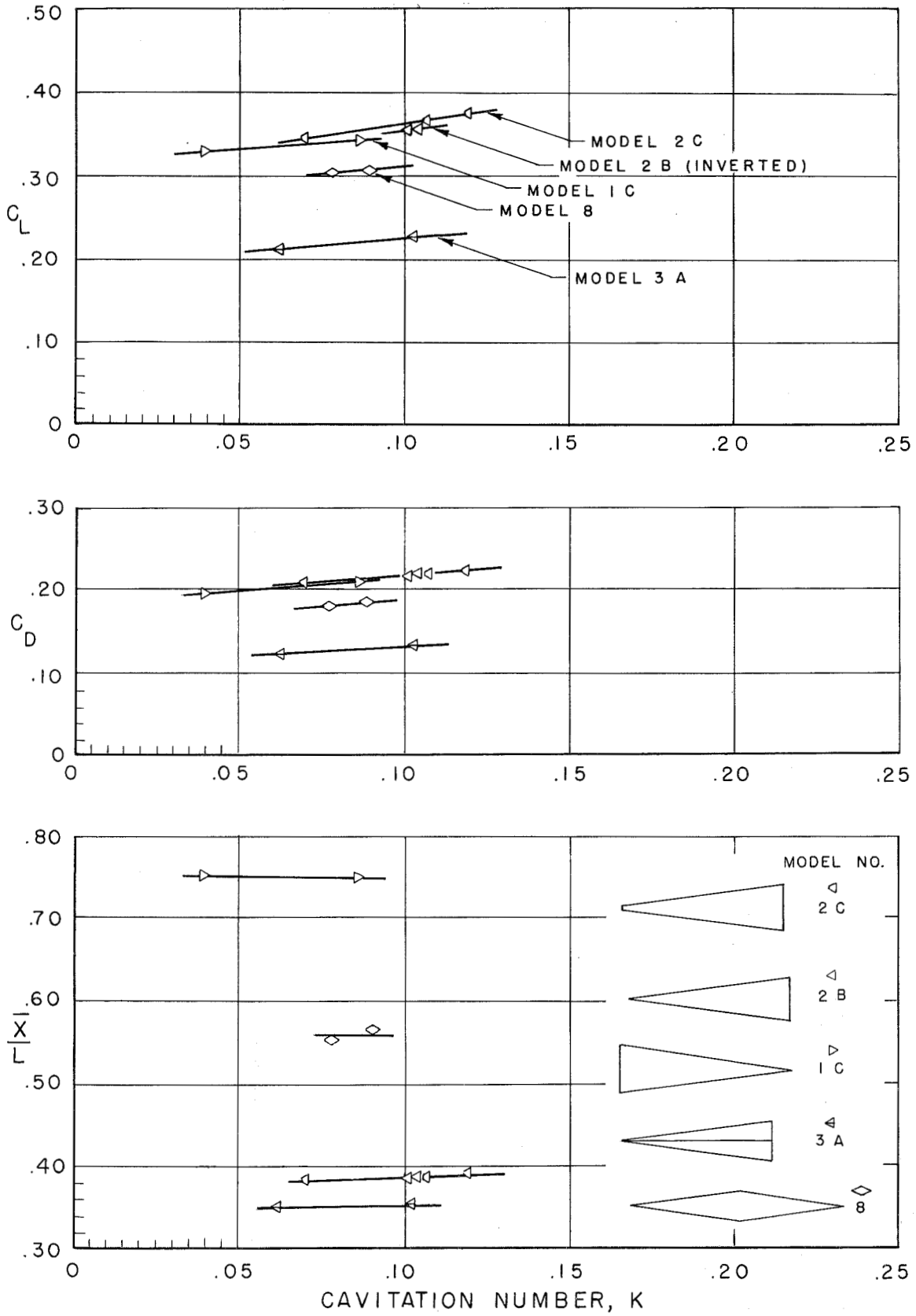

Fig. 17 - Lift, Drag and Center of Pressure Location for Various Superventilated Delta Wings at an Angle of Attack of 30°. Model descriptions are given in Fig. 3. Flow is from left to right for models as shown.

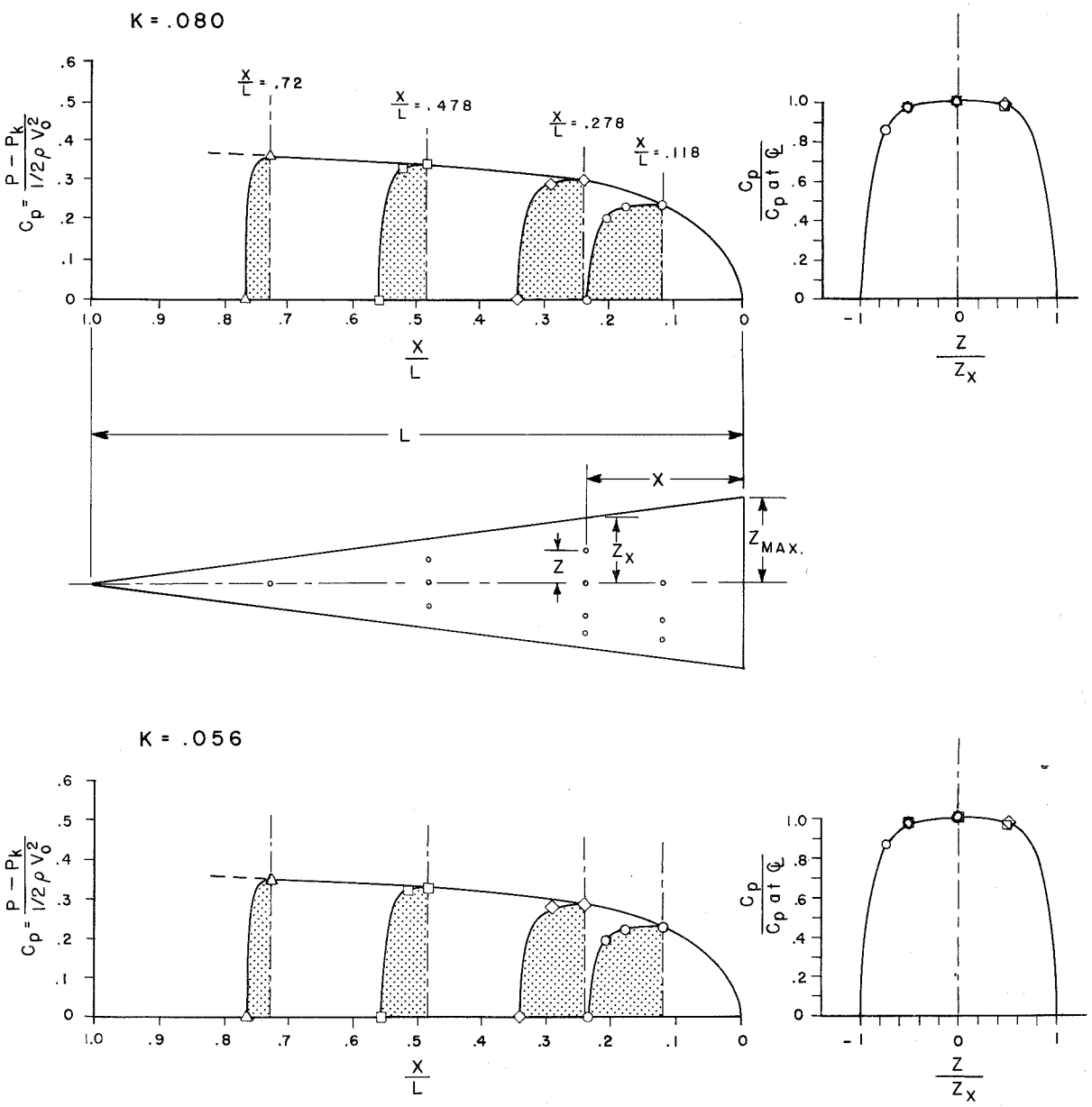

Fig. 18 - Pressure Distribution of a 15° Superventilated Delta Wing at 21° Angle of Attack.

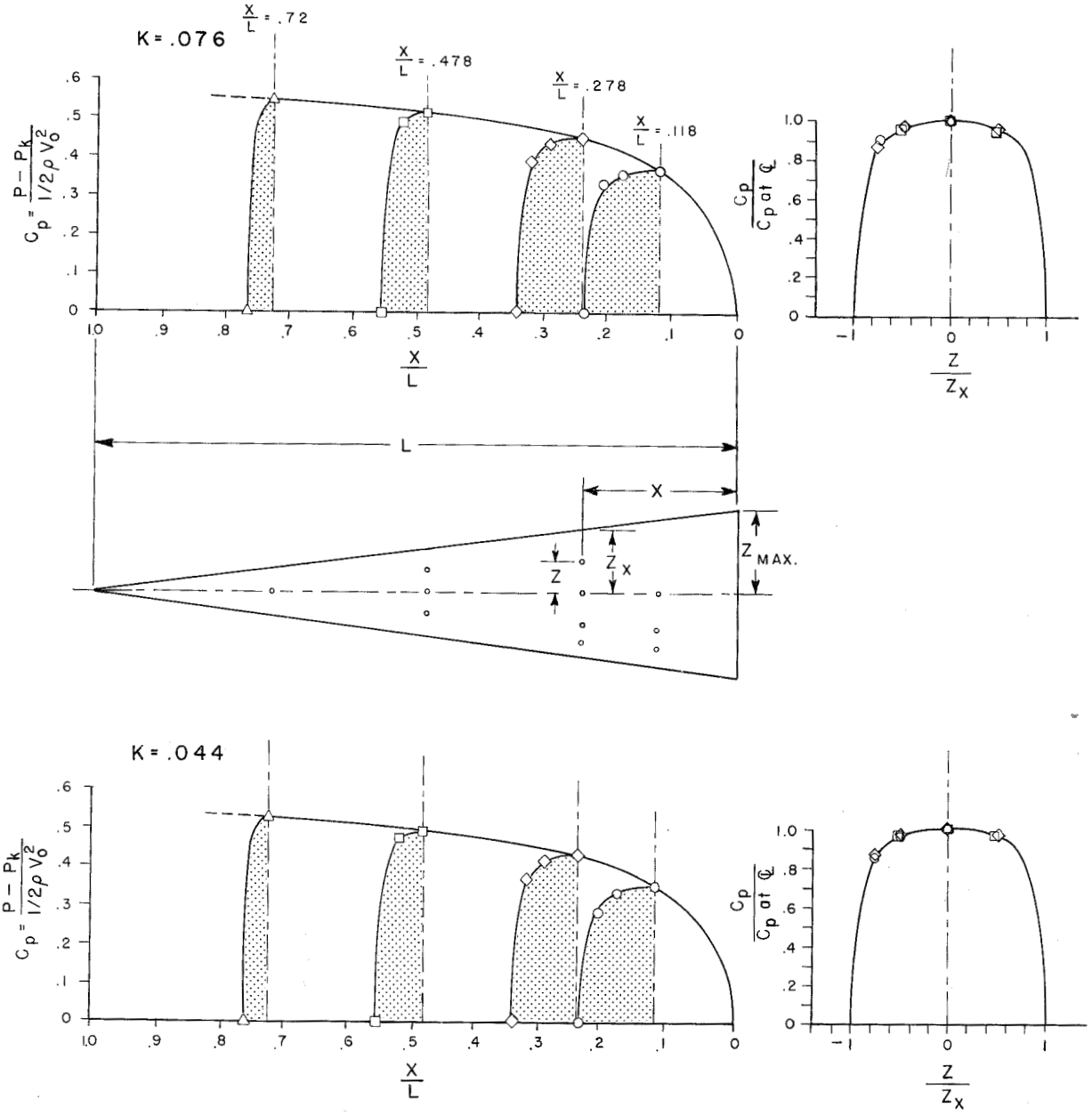

Fig. 19 - Pressure Distribution of a 15° Superventilated Delta Wing at 30° Angle of Attack.

APPENDIX I

SUMMARY OF FORCE DATA

Model Designation	γ	A ft^2	α	Y*	K	$\frac{V_o^2}{2g}$	C_L	C_D	$\frac{\bar{x}}{L}$
9	10°	.06016	30°	.553	.073	5.120	.324	.1921	.366
			30°	.553	.114	5.140	.344	.2055	.369
			30°	.553	.107	5.146	.340	.2033	.370
			25°	.576	.062	5.275	.269	.1288	.362
			25°	.576	.100	5.370	.291	.1406	.366
			21°	.595	.055	5.117	.226	.0899	.369
			21°	.595	.058	5.217	.225	.0898	.368
			30°	.553	.107	5.150	.343	.2044	.366
			30°	.553	.073	5.190	.324	.1926	.366
			20°	.599	.051	5.333	.206	.0777	.363
2	15°	.1158	30°	.639	.117	2.980	.356	.21237	-
			30°	.639	.194	2.970	.405	.24056	-
			30°	.639	.160	2.990	.384	.22531	-
			30°	.639	.136	3.000	.370	.22147	-
3	15°	.0585	30°	.580	.070	5.130	.332	.1966	.369
			30°	.580	.073	5.150	.331	.1959	.368
			30°	.580	.083	5.160	.338	.1995	.362
			30°	.580	.087	5.170	.338	.1991	.363
			30°	.580	.122	5.150	.359	.2132	.370
			30°	.580	.125	5.180	.359	.2127	.367
3	15°	.0585	21°	.615	.045	5.120	.235	.0947	.373
			21°	.415	.048	5.125	.227	.0914	.378
			21°	.215	.042	5.130	.222	.0885	.376
			21°	.115	.026	5.140	.217	.0870	.380
			21°	.090	.018	5.120	.214	.0855	.374
3	15°	.0585	21°	.615	.040	9.400	.232	.0937	.362
3	15°	.0585	30°	.198	.039	5.125	.317	.188	.377
			30°	.248	.052	5.120	.318	.188	.376
			30°	.298	.058	5.110	.323	.191	.373
			30°	.398	.078	5.080	.329	.195	.375
			30°	.498	.093	5.100	.349	.207	.375
3	15°	.0585	25°	.164	.032	5.150	.260	.124	.377
			25°	.214	.043	5.150	.263	.126	.375
			25°	.264	.050	5.110	.265	.126	.376
			25°	.292	.051	5.130	.273	.128	.376

APPENDIX I

(continued)

Model Designation	γ	A ft^2	α	Y*	K	$\frac{V_o^2}{2g}$	C_L	C_D	$\frac{\bar{x}}{L}$
3	15^o	.0585	20^o	.138	.027	5.110	.205	.080	.379
			20^o	.188	.035	5.110	.210	.082	.379
			20^o	.197	.037	5.110	.210	.082	.379
3	15^o	.0585	21^o	.137	.052	2.415	.229	.094	.378
			21^o	.137	.024	5.275	.216	.088	.382
			21^o	.143	.028	5.130	.217	.089	.378
			21^o	.143	.021	6.740	.211	.087	.383
			21^o	.193	.030	7.050	.216	.089	.376
			21^o	.193	.038	5.060	.219	.091	.378
			21^o	.193	.047	3.860	.225	.093	.377
			21^o	.193	.068	2.380	.236	.095	.369
3	15^o	.0585	10^o	.058	.024	2.460	.100	.022	.371
			10^o	.058	.015	3.750	.091	.021	.377
			10^o	.058	.011	5.250	.088	.020	.378
			10^o	.058	.008	7.130	.087	.020	.381
			10^o	.069	.010	7.130	.088	.020	.384
			10^o	.069	.013	5.270	.093	.022	.384
			10^o	.069	.008	8.075	.088	.020	.382
3	15^o	.0585	25^o	.600	.112	1.690	.311	.147	.347
			25^o	.500	.107	1.685	.307	.147	.355
			25^o	.400	.106	1.690	.304	.146	.358
			25^o	.300	.101	1.700	.296	.142	.355
			25^o	.200	.098	1.680	.297	.143	.362
			25^o	.154	.091	1.700	.291	.140	.366
			25^o	.250	.154	1.620	.350	.172	.374
			25^o	.200	.145	1.650	.324	.158	.369
			25^o	.158	.093	1.640	.298	.144	.367
			25^o	.600	.062	5.260	.280	.134	.368
			25^o	.500	.055	5.220	.276	.133	.373
			25^o	.350	.052	5.230	.272	.131	.380
			25^o	.250	.044	5.220	.269	.129	.373
			25^o	.166	.032	5.235	.264	.127	.368
			25^o	.600	.113	5.360	.318	.158	.375
			25^o	.450	.099	5.360	.303	.150	.382
			25^o	.400	.091	5.390	.298	.146	.380
			25^o	.250	.078	5.370	.285	.139	.382
			25^o	.210	.064	5.340	.277	.135	.381
			25^o	.194	.041	5.320	.266	.129	.378
			25^o	.168	.032	5.310	.261	.127	.379
			25^o	.600	.089	9.110	.304	.151	.374

APPENDIX I

(continued)

Model Designation	γ	A ft^2	α	Y*	K	$\frac{V_o^2}{2g}$	C_L	C_D	$\frac{\bar{x}}{L}$
3	15°	.0585	25°	.500	.087	9.110	.296	.148	.385
			25°	.400	.081	9.180	.289	.143	.381
			25°	.300	.067	9.255	.281	.139	.382
			25°	.250	.058	9.350	.278	.137	.380
			25°	.300	.067	9.350	.281	.138	.381
			25°	.250	.057	9.400	.277	.136	.380
			25°	.168	.017	9.250	.260	.128	.382
			25°	.600	.047	9.340	.279	.136	.377
			25°	.450	.043	9.330	.276	.134	.378
			25°	.300	.035	9.200	.268	.132	.376
	15°	.0585	25°	.166	.018	9.110	.260	.128	.382
2A	15°	.0605	30°	.553	.088	3.620	.344	.2036	.371
			30°	.553	.149	3.620	.386	.2314	.371
			30°	.553	.138	3.620	.373	.2224	.369
			30°	.553	.119	3.630	.359	.2138	.368
			30°	.553	.089	3.630	.344	.2042	.368
2A	15°	.0605	21°	.598	.060	3.66	.240	.096	.360
			21°	.598	.067	3.64	.243	.098	.359
			21°	.598	.084	3.56	.252	.105	.374
			21°	.598					
			21°	.598	.054	5.12	.234	.095	.375
7	30°	.0563	30°	.609	.070	5.210	.365	.214	.382
			30°	.609	.082	5.280	.367	.216	.385
			30°	.609	.101	3.070	.379	.222	.381
			25°	.609	.059	5.220	.320	.155	.388
			25°	.609	.108	5.220	.344	.169	.391
			25°	.609	.076	3.000	.329	.158	.380
4	45°	.0582	30°	.621	.128	5.180	.417	.249	.390
			30°	.621	.074	5.180	.404	.240	.394
			30°	.521	.133	5.200	.416	.249	.395
			30°	.521	.065	5.260	.385	.228	.386
4	45°	.0582	30°	.621	.125	5.210	.412	.242	.399
			30°	.621	.071	5.280	.386	.226	.399
			30°	.621	.100	5.200	.393	.230	.391

APPENDIX I

(continued)

Model Designation	γ	A ft^2	α	Y*	K	$\frac{V_o^2}{2g}$	C_L	C_D	$\frac{\bar{x}}{L}$
4	45^o	.0582	30^o	.621	.077	5.100	.388	.230	.396
			30^o	.621	.092	5.100	.394	.234	.399
			30^o	.621	.149	5.100	.404	.241	.405
			30^o	.621	.158	5.080	.393	.234	.403
4	45^o	.0582	30^o	.621	.103	3.030	.405	.237	.388
			30^o	.621	.119	3.020	.410	.242	.392
			30^o	.471	.094	3.030	.393	.233	.398
			30^o	.321	.112	3.030	.410	.238	.397
			30^o	.621	.068	5.100	.390	.230	.400
4	45^o	.0582	25^o	.634	.119	5.180	.372	.182	.403
			25^o	.634	.070	5.220	.348	.169	.399
			25^o	.634	.096	5.240	.359	.175	.397
			25^o	.157	.125	5.300	.328	.159	.401
4	45^o	.0582	25^o	.634	.095	2.935	.360	.173	.386
			25^o	.634	.080	2.940	.351	.168	.382
			25^o	.284	.067	2.750	.336	.162	.396
			25^o	.234	.061	2.760	.334	.161	.400
			25^o	.153	.048	2.790	.329	.158	.395
6	60^o	.06415	30^o	.626	.111	5.200	.423	.250	.408
			30^o	.626	.073	5.230	.406	.240	.414
6	60^o	.06415	30^o	.626	.114	5.210	.427	.250	.392
			30^o	.626	.071	5.300	.408	.238	.395
			25^o	.635	.065	5.145	.366	.163	-
			25^o	.635	.116	5.240	.390	.189	.382
5	90^o	.0625	30.3^o	.640	.074	5.100	.446	.266	.392
			30.3^o	.640	.115	5.120	.469	.282	.397
			30^o	.640	.075	5.120	.446	.262	.382
			30^o	.640	.114	5.150	.464	.275	.396
			30^o	.640	.100	2.910	.457	.267	.371
			30^o	.640	.130	2.910	.469	.276	.385
			30^o	.640	.073	5.130	.442	.260	.387
			30^o	.440	.068	5.140	.438	.259	.390
			30^o	.340	.074	5.150	.438	.259	.390
			30^o	.240	.071	5.200	.442	.262	.396
			30^o	.090	.017	5.190	.426	.252	.395

APPENDIX I

(continued)

Model Designation	γ	A ft^2	α	Y*	K	$\frac{V_o^2}{2g}$	C_L	C_D	$\frac{\bar{x}}{L}$
8	15^o	.0544	30^o	.670	.0777	5.210	.300	.176	.553
			30^o	.670	.0892	5.270	.308	.181	.567
1C	15^o	.06292	30^o	.449	.0390	5.230	.326	.194	.751
			30^o	.449	.0861	5.230	.342	.205	.750
2C	15^o	.0583	30^o	.556	.0696	5.190	.345	.203	.385
			30^o	.556	.1067	5.210	.366	.217	.388
			30^o	.556	.1190	5.260	.372	.221	.389
2B	15^o	.0601	30^o	.703	.104	4.450	.355	.216	.388
			30^o	.603	.101	4.490	.353	.213	.385
3A	15^o	.0479	30^o	.589	.062	5.190	.212	.124	.353
			30^o	.589	.102	5.260	.230	.134	.357

APPENDIX II
Summary of Pressure Data

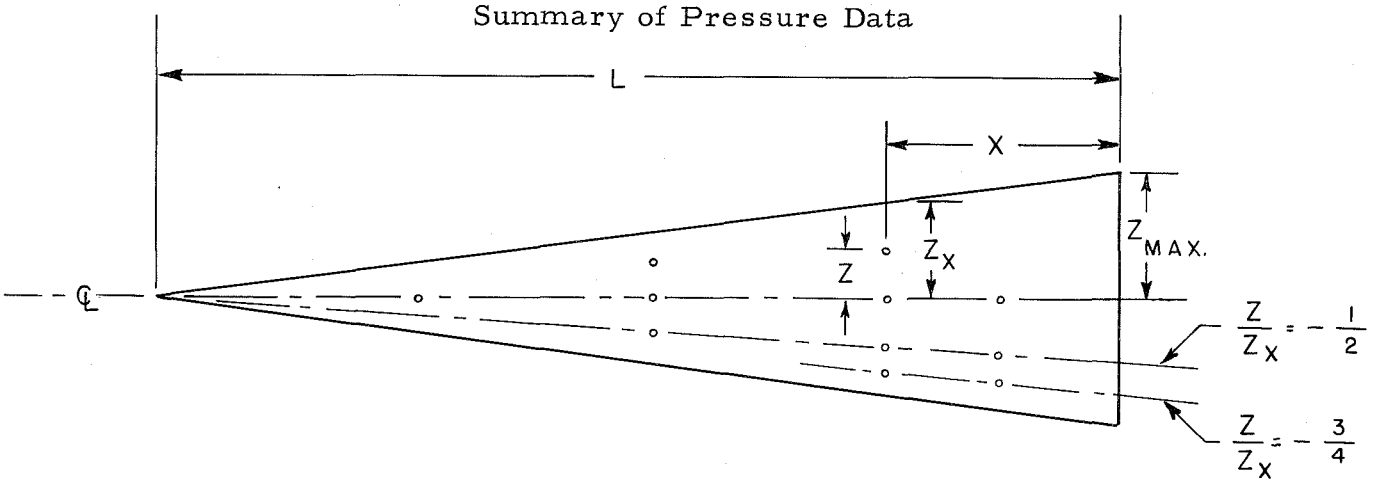

Apex Angle, $\gamma = 15^\circ$

Velocity = 18.5 fps

Pressure Tap No.

	K	①	②	③	④	⑤	⑥	⑦	⑧	⑨	⑩	⑪
$\frac{x}{L}$		.72	.478	.478	.478	.238	.238	.238	.238	.118	.118	.118
$\frac{z}{z_x}$		0	.488	0	-.522	.512	0	-.500	-.760	0	-.500	-.752
$\frac{z}{z_{max}}$		0	.254	0	-.272	.390	0	-.382	-.580	0	-.440	-.664

Angle of Attack, $\alpha = 30^\circ$

c_p	.076	.540	.489	.514	.488	.438	.449	.434	.387	.369	.356	.332
$\frac{c_p}{c_p @ ℄}$	.076	1.000	.952	1.000	.949	.975	1.000	.966	.862	1.000	.965	.900

Angle of Attack, $\alpha = 30^\circ$

c_p	.044	.526	.470	.486	.471	.418	.428	.413	.370	.348	.336	.299
$\frac{c_p}{c_p @ ℄}$	.044	1.000	.966	1.000	.969	.975	1.000	.964	.864	1.000	.965	.859

Angle of Attack, $\alpha = 21^\circ$

c_p	.080	.363	.332	.344	.335	.296	.302	.294	.292	.240	.234	.208
$\frac{c_p}{c_p @ ℄}$	.080	1.000	.967	1.000	.973	.978	1.000	.972	.968	1.000	.973	.866

Angle of Attack, $\alpha = 21^\circ$

c_p	.056	.347	.316	.327	.318	.282	.288	.279	.298	.227	.222	.196
$\frac{c_p}{c_p @ ℄}$	.056	1.000	.967	1.000	.971	.980	1.000	.970	.967	1.000	.975	.862

DISTRIBUTION LIST

Chief, Bureau of Naval Weapons
Department of the Navy
Washington 25, D.C.
Attn: Codes DLI-3 (1)
RAAD-3 (1)
RRRE (1)
RRRE-7 (1)
RUAW-4 (2)

Chief, Bureau of Ships
Department of the Navy
Washington 25, D.C.
Attn: Codes 335 (1)
421 (2)
442 (1)
644 (1)

Chief of Naval Research
Department of the Navy
Washington 25, D.C.
Attn: Codes 429 (1)
438 (1)
466 (1)

Commanding Officer and Director
David Taylor Model Basin
Washington 7, D.C.
Attn: Codes 142 (1)
500 (1)
526 (1)
591 (1)

Chief, Bureau of Yards and Docks
Department of the Navy
Washington 25, D.C.
Attn: Research Division (1)

Commanding Officer and Director
U.S. Naval Engrg. Experiment Sta.
Annapolis, Maryland
Attn: Librarian (1)

Superintendent
U.S. Naval Academy
Annapolis, Maryland
Attn: Librarian (1)

Superintendent
U.S. Naval Postgraduate School
Monterey, California
Attn: Librarian (1)

Commander
U.S. Naval Weapons Laboratory
Dahlgren, Virginia
Attn: Librarian (1)

Commanding Officer
U.S. Naval Underwater Ord. Sta.
Newport, Rhode Island
Attn: Librarian (1)

Commander
U.S. Naval Ordnance Laboratory
White Oak, Silver Spring, Md.
Attn: Desk DL (Library) (1)
XL (Aeroballistics) (1)

Commanding Officer and Director
U.S. Naval Civil Engrg. Laboratory
Port Hueneme, California
Attn: Librarian (1)

Commander
U.S. Naval Ordnance Test Station
Pasadena Annex
3202 E. Foothill Blvd.
Pasadena, California
Attn: Codes P508 (2)
P804 (2)
P8074 (1)
P8076 (1)
P80962 (1)

Director
Naval Research Laboratory
Washington 25, D.C.
Attn: Librarian (1)

Commanding Officer and Director
U.S. Navy Underwater Sound Lab.
Fort Trumbull
New London, Connecticut
Attn: Librarian (1)

Commanding Officer and Director
U.S. Navy Electronics Laboratory
San Diego 52, California
Attn: Librarian (1)

Commanding Officer and Director
U.S. Naval Air Developmt. Center
Johnsville, Pennsylvania
Attn: Librarian (1)

Commanding Officer
U.S. Navy Mine Defense Lab.
Panama City, Florida
Attn: Librarian (1)

Commander
U.S. Naval Ordnance Test Station
China Lake, California
Attn: Code 7533 (1)

British Joint Services Mission
(Navy Staff), via
Chief, Bureau of Naval Weapons
Department of the Navy
Washington 25, D.C.
Attn: Code DSC-3 (4)

Defense Research Member (W)
Canadian Joint Staff, via
Chief, Bureau of Naval Weapons
Department of the Navy
Washington 25, D.C.
Attn: Code DSC-3 (1)

ASTIA Reference Center
Technical Information Division
Library of Congress
Washington 25, D.C. (1)

Defense Documentation Center
Cameron Station
Alexandria, Virginia (6)

Office of Technical Services
Department of Commerce
Washington, D.C. (1)

Scientific and Technical Information
Facility
Attn: NASA Representative
P.O. Box 5700
Bethesda, Maryland 20014

Director
National Bureau of Standards
Washington 25, D.C.
Attn: Fluid Mechanics Div. (1)

Coordinator for Research
Maritime Administration
441 G Street, N.W.
Washington, D.C. (1)

Director
Engineering Sciences Division
National Science Foundation
1520 H Street, N.W.
Washington, D.C. (1)

Commander
Air Research and Developmt. Command
Andrews Air Force Base
Washington 25, D.C. (1)

Air Force Office of Scient. Research
Mechanics Division
Washington 25, D.C. (1)

Commanding Officer
Office of Ordnance Research
Box CM, Duke Station
Durham, North Carolina (1)

Committee on Undersea Warfare
Nat. Academy of Sciences
National Research Council
2101 Constitution Avenue, N.W.
Washington 25, D.C. (1)

Director
U.S. Army Engineer Waterways
Experiment Station
Corps of Engineers
Vicksburg, Mississippi (1)

Superintendent
U.S. Merchant Marine Academy
Kings Point, Long Island, N.Y.
Attn: Librarian (1)

Massachusetts Institute of Tech.
Cambridge 39, Mass.
Attn: Dept. of Naval Architecture
and Marine Engineering
Prof. L. Troost (1)
Hydrodynamics Laboratory
Prof. A. Ippen (1)

Applied Physics Laboratory
University of Washington
Seattle, Washington
Attn: Librarian (1)

Director
St. Anthony Falls Hydraulic Lab.
University of Minnesota
Minneapolis 14, Minn. (1)

Stanford University
Stanford, California
Attn: Dept. of Mechanical Engrg.
Prof. B. Perry (1)
Head, Dept. of Math. (1)

Cornell University
Ithaca, New York
Attn: Director, Graduate School
of Aeronautical Engrg. (1)

Harvard University
Cambridge 38, Massachusetts
Attn: Dept. of Engineering Sciences
Prof. G.F. Carrier (1)
Dept. of Mathematics
Prof. G. Birkhoff (1)

Iowa Institute of Hydraulic Research
State University of Iowa
Iowa City, Iowa
Attn: Prof. H. Rouse, Dir. (1)
Prof. L. Landweber (1)

Director
Alden Hydraulic Laboratory
Worcester Polytechnic Institute
Worcester, Massachusetts (1)

University of Arizona
Department of Mathematics
Tucson, Arizona
Attn: Prof. L.M. Milne-Thomson
(1)

Director
Garfield Thomas Water Tunnel
Ordnance Research Laboratory
Pennsylvania State University
P.O. Box 30
University Park, Pa. (1)

Davidson Laboratory
Stevens Institute of Technology
711 Hudson Street
Hoboken, New Jersey
Attn: Dr. J. Breslin (1)

Johns Hopkins University
Baltimore 18, Maryland
Attn: Prof. S. Corrsin, Head
Dept. of Mech. Engrg. (1)

Colorado State University
Fort Collins, Colorado
Attn: Prof. M. Albertson
Dept. of Civil Engrg. (1)

University of Michigan
Ann Arbor, Michigan
Attn: Prof. R.B. Couch (1)
Prof. V. Streeter (1)

Polytechnic Institute of Brooklyn
99 Livingston Street
Brooklyn 2, New York
Attn: Head, Dept. of Aero. Eng.
and Applied Mech. (1)

Brown University
Providence, Rhode Island
Attn: Div. of Applied Math. (1)
Div. of Engineering (1)

University of California
Berkeley 4, California
Attn: College of Engineering
Prof. A. Schade (1)
Prof. I.V. Wehausen (1)

Webb Institute of Naval Architecture
Crescent Beach Road
Glen Cove, Long Island, N.Y.
Attn: Librarian (1)

New York State Maritime College
Fort Schuyler, New York
Attn: Librarian (1)

University of Kansas
Lawrence, Kansas
Attn: Dean J.S. McNown (1)

Lehigh University
Bethlehem, Pennsylvania
Attn: Prof. J.B. Herbich
Civil Engrg. Dept. (1)

University of Notre Dame
Notre Dame, Indiana
Attn: Prof. A.G. Strandhagen (1)
Dept. of Engineering Mech.

Rensselaer Polytechnic Institute
Troy, New York
Attn: Prof. H. Cohen
Dept. of Mathematics (1)

California Institute of Technology
Pasadena, California
Attn: Prof. F.C. Lindvall (1)
Prof. M.S. Plesset (1)

University of Illinois
Urbana, Illinois
Attn: College of Engineering
Prof. J. Robertson (1)

Scripps Institution of Oceanography
University of California
La Jolla, California
Attn: Librarian (1)

Woods Hole Oceanographic Institute
Woods Hole, Massachusetts
Attn: Librarian (1)

Case Institute of Technology
Cleveland, Ohio
Attn: Librarian (1)

Institute of Fluid Mechanics
and Applied Mechanics
University of Maryland
College Park, Md.
Attn: Librarian (1)

Yale University
Mason Laboratory
400 Temple Street
New Haven 10, Connecticut
Attn: Librarian (1)

Philco Corporation
4700 Wissahickon Avenue
Philadelphia, Pennsylvania
Attn: Engrg. Librarian (1)

Vitro Corporation of America
962 Wayne Avenue
Silver Springs, Maryland
Attn: Engrg. Librarian (1)

Gibbs and Cox
21 West Street
New York 6, N.Y.
Attn: Dr. S. Hoerner (1)

Hydronautics, Inc.
Pindell School Road
Howard County
Laurel, Md.
Attn: Mr. P. Eisenberg (1)

Technical Research Group
Route 110
Melville, N.Y.
Attn: Librarian (1)

Aerojet General Corporation
6352 North Irwindale Avenue
Azusa, California
Attn: Mr. J. Levy (1)

The Martin Company
Baltimore 3, Maryland
Attn: Science Tech. Librarian
Mail No. J398 (1)

North American Aviation, Inc.
International Airport
Los Angeles 45, California
Attn: Engineering Librarian
Dept. 56 (1)

Lockheed Aircraft Corporation
1555 N. Hollywood Way
Burbank, California
Attn: Engineering Librarian
Bldg. 63, Factory A1 (1)

Douglas Aircraft Company, Inc.
El Segundo, California
Attn: Mr. A.M.O. Smith (1)

Bell Aerosystem Company
P.O. Box 1
Buffalo 5, New York
Attn: Engineering Librarian (1)

McDonnell Aircraft Corporation
P.O. Box 516
St. Louis 3, Missouri
Attn: Engineering Librarian (1)

Chance Vought Aircraft, Inc.
P.O. Box 5907
Dallas 22, Texas
Attn: Engineering Library (1)

Republic Aviation Corporation
Farmingdale, Long Island, N.Y.
Attn: Engineering Librarian (1)

EDO Corporation
College Point, New York
Attn: Engineering Librarian (1)

The RAND Corporation
1700 Main Street
Santa Monica, California
Attn: Librarian (1)

Electric Boat Division
General Dynamics Corporation
Groton, Connecticut
Attn: Engineering Librarian (1)

Hydrodynamics Laboratory
Convair Division
General Dynamics Corporation
P.O. Box 1950
San Diego 12, California
Attn: Mr. H.E. Brooke (1)

Goodyear Aircraft Company
Akron 15, Ohio
Attn: Engineering Librarian (1)

Grumman Aircraft Engrg. Corp.
Bethpage, Long Island, N.Y.
Attn: Engineering Librarian
Plant 5 (1)

Aeronutronic Division
Ford Motor Company
Ford Road
Newport Beach, California
Attn: Engineering Librarian (1)

Director
Department of Applied Mechanics
Southwest Research Institute
8500 Culebra Road
San Antonio 6, Texas (1)

Boeing Airplane Company
P.O. Box 3707
Seattle, Washington
Attn: Aero-Space Div. Librarian
Org. No. 2-5190, Mail
Stop 1384 (1)

Hughes Tool Company
Florence and Trole
Culver City, California
Attn: Librarian Bldg. 2
Mail Station 5 (1)

United Technology Corporation
P.O. Box 358
Sunnyvale, California
Attn: Dr. D.A. Rains (1)

Cleveland Pneumatic Ind., Inc.
Adv. Systems Development Div.
1301 El Segundo Blvd.
El Segundo, California
Attn: Mr. S. Thurston (1)
Mr. W. Ellsworth (1)

Westinghouse Electric Corp.
Baltimore Division
P.O. Box 1897
Friendship International Airport, Md.
Attn: Engineering Librarian (1)

General Electric Corporation
Ordnance Department
100 Plastics Ave.
Pittsfield, Massachusetts
Attn: Engineering Librarian (1)

Society of Naval Architects and
Marine Engineers
74 Trinity Place
New York 6, N.Y. (1)

Applied Mechanics Reviews
American Soc. of Mech. Engineers
29 West 39th Street
New York, N.Y. (1)

Engineering Societies Library
29 West 39th Street
New York 18, N.Y. (1)

Oceanics, Inc.
Technical Industrial Park
Plainview, Long Island, N.Y.
Attn: Dr. P. Kaplan (1)

General Electric Corporation
LME Dept., Bldg. 28
No. 1 River Road
Schenectady 5, New York
Attn: Engineering Librarian (1)

Clevite Brush Development
Clevite Research Center
540 E. 105th Street
Cleveland, Ohio
Attn: Engineering Librarian (1)

AVCO Manufacturing Company
2385 Revere Beach Parkway
Everett 49, Massachusetts
Attn: Engineering Librarian (1)

Inst. of the Aerospace Sciences Library
2 East 64th Street
New York 21, N.Y. (1)

New York Naval Shipyard
Material Laboratory
Brooklyn, N.Y.
Attn: Mr. D. Kallas (2)

Laboratorio Hidrotecnico
Salturnino de Brito
Rua Ferreira Pontes 637
Rio de Janeiro, Brazil
Attn: Mr. V.F. Motta (1)

Commander
Office of Naval Research
USN, Fluid Dynamics Branch
Washington 25, D.C.
Mr. A.J. Coyle (6)